Studies on the Ice Sheet Flow and Local Mass Budget in Mizuho Plateau, Antarctica*

by

Renji NARUSE
成瀬廉二
The Institute of Low Temperature Science

Received December 1978

Abstract

Surveys of a triangulation chain 250 km in length were carried out in 1969 and 1973-1974 along the parallel of 72°S in Mizuho Plateau, East Antarctica. Obtained from them were horizontal and vertical components of surface velocities of the ice sheet at 140 stations and parameters of surface strains at 140 triangles of the chain. Local mass budgets at the triangulation stations were deduced from vertical velocities and accumulation rates. General dynamic conditions over Mizuho Plateau were also discussed.

Horizontal velocities were small near the Yamato Mountains, while they had the maximum more than 20 ± 0.7 m a^{-1} around 39°E. The direction of the flow vector was, in general, identical approximately with that of the large-scale maximum slope of the ice surface. Tensile strains predominated mostly over compressive strains, and the direction of the maximum extension was rather close to that of the ice flow. Submergence velocities indicated large values, such as -0.7 to -1 ± 0.25 m a^{-1}, in the region from 39°E eastward. The amount of snow accumulation was not enough in this region to compensate for the deficit of the ice mass caused by the submergence flow. It followed that the local mass budget was negative there. It is suggested from this study that the ice sheet of Mizuho Plateau is in an unsteady state as a whole.

* Contribution No. 1992 from the Institute of Low Temperature Science.
北海道大学審査学位論文

Contents

I. Introduction 3
II. Method of survey and reduction of observed data 4
II. 1. Outline of the triangulation chain 4
II. 2. Procedure of survey 5
II. 3. Measurement of distance 7
II. 4. Computation of position 8
II. 5. Computation of elevation 9
III. Calculation of flow vector and strain 11
III. 1. Horizontal component of surface velocity 11
III. 2. Emergence or submergence velocity 15
III. 3. Strain rate of the ice sheet surface 16
IV. Distribution of horizontal flow velocity and surface strain 22
IV. 1. Distribution of flow vector and principal strain 22
IV. 2. Variations in flow velocity, dilatation, maximum shear strain, and rotation 25
V. Relation between horizontal flow and topography 27
V. 1. Classification of surface features 27
V. 2. Relation between directions of surface slope and flow 30
V. 3. Profile of bedrock relief 31
V. 4. Empirical relation of surface velocity 34
VI. Vertical flow and local mass budget deduced from it 36
VI. 1. Distribution of annual net accumulation 36
VI. 2. Variation in emergence or submergence velocity 37
VI. 3. Local mass budget at each triangulation station 38
VII. Conditions of ice flow over Mizuho Plateau 41
VII. 1. Distribution of strains measured by square strain grids 41
VII. 2. Local mass budget deduced from strain measurement 43
VII. 3. Estimated velocities and flow lines 45
VIII. Concluding remarks 48
Acknowledgements 50
References 50

I. Introduction

Accurate information is much sought on the flow of the Antarctic ice sheet in the studies of such problems as its present stability, its response to a climatic change, and the physical behaviour of a large ice mass in general. Direct measurements of the flow have, however, been made intensively only in limited regions near the coast and on ice shelves ; for example, in the Mawson area (MELLOR 1959a), in the Amery Ice Shelf (BUDD 1966), in the Wilkes local ice cap (BUDD 1968), in the Ross Ice Shelf (SWITHINBANK 1968, DORRER *et al.* 1969, THOMAS and EILERS 1975) and in Sôya Coast (AGETA and NARUSE 1971, FUJIWARA and YOSHIDA 1972, SHIMIZU *et al.* 1975). Difficulties in selecting permanent datum points, i. e. nunataks, constitute an unfavourable condition for conducting a geodetic survey in the inland regions. Some measurements of the flow not referring to bare rocks were tried at various ice caps and ice sheets by measuring a strain net on the assumption that horizontal velocity should be zero at the ice divide (WHILLANS 1973, DOAKE *et al.* 1976), or analyzing radio-echo fading patterns due to the roughness of a glacier bed (NYE *et al.* 1972, WALFORD 1972, DOAKE 1975). Being in the developing stage, however, they have presented some problems in determining accurate velocities.

A study on the ice sheet flow was one of the main subjects of the Japanese Glaciological Research Program (SHIMIZU 1978) conducted in 1969-1975 over the ice sheet of Mizuho Plateau, East Antarctica. For this study, during a period from 24 November to 30 December 1969 the traverse party of the 10th Japanese Antarctic Research Expedition (JARE-10) set up a triangulation chain over a distance of 250 km in the inland region of Mizuho Plateau, starting at the Yamato Mountains (NARUSE *et al.* 1972). The chain was composed of 164 stations, forming a series of triangles totaling 162. The second survey was carried out four years later during a period from 20 December 1973 to 16 January 1974 by JARE-14 (NARUSE 1975a). Measurements were also made along the chain as to the surface elevation, ice thickness (SHIMIZU *et al.* 1972, NARUSE and YOKOYAMA 1975), surface slope (NARUSE 1975a), net accumulation (YOKOYAMA 1975), surface meteorological data (AGETA and FUKUSHIMA 1972, KOBAYASHI 1975), gravity and geomagnetism (YOSHIDA and YOSHIMURA 1972a, b, ABE 1975a, b). Besides the chain, nine square strain grids were set up in 1969-1970 (NARUSE *et al.* 1972) in various points of Mizuho Plateau and seven of them were resurveyed until 1975 (SATOW 1977).

Despite that the survey of a triangulation chain requires laborious work, it has three major advantages, compared with a commonly employed traverse survey, for the research of a surface flow on the far-spreading ice sheet. Firstly, one can check and correct an observational error at an individual triangle of the chain *in situ* ; accordingly, the total error accumulated throughout the survey can be controlled within a much smaller range than is possible in a traverse survey. For this reason, it allows to set up a long chain in an inland region far from an ice-free rock. Secondly, the results of the geodetic position of each station calculated by applying the

least squares method should have higher accuracies in the survey of the chain than in that of a traverse, since the former allows by far the more numbers of angle and distance measurements than the latter. Thirdly, the survey of the triangulation chain provides information of not only the velocity of an ice flow, but also the surface strain rate of each triangle.

In the present paper, procedures of triangulation surveys and methods of data reduction and calculation are first described in Sections II and III. Next, the reduced data such as the horizontal velocity of surface flow and the parameters of surface strain are presented in Sections IV and V, together with some discussions of their distribution over the surveyed region and of the relation between them and the ice sheet topography. Then, in Section VI, a new concept of "local mass budget" or "mass budget density", the integration of which over an area gives the total mass budget of the area, is introduced and its values at the surveyed points are deduced from vertical velocities. The author believes it natural that several vague estimations of the total mass budget of the Antarctic ice sheet (e. g., MELLOR 1959b, LOEWE 1967, GIOVINETTO 1968, BARDIN and SUYETOVA 1969) should be substituted by accurate estimations based on this concept, if such estimations are to be used for discussing the stability of the ice sheet. With this belief in mind, the dynamic condition of the ice sheet in Mizuho Plateau is discussed in Section VII.

II. Method of survey and reduction of observed data

II. 1. *Outline of the triangulation chain*

The triangulation chain stretched along the parallel of 72°S for a total distance of 250 km between A001 at the southeast end of the Yamato Mountains and A164 (S240), as shown in Fig. 1. Composed of 164 stations, the chain formed a series of 162 triangles, as illustrated in Fig. 2. The surface elevation of the ice sheet increased gradually along the chain from 2250 m near A001 to 2600 m near A164, so the chain may be considered approximately parallel to a surface contour line.

The datum point of the triangulation chain, A001, was selected up on Motoi nunatak, which belongs to the Yamato Mountains. Positions and elevations of all the triangulation stations were determined in reference to their values at the datum point. The adopted position of this point was 71°47′28.1″S in latitude and 36°12′12.2″E in longitude obtained by the astronomic observation carried out in 1969, while the adopted elevation was 2254 m obtained by the barometric method in 1969-1970 (SHIMIZU *et al.* 1972). The base line of the chain was established between A001 and the neighbouring ice-free rock A002.

The lengths of triangle sides differed considerably from place to place depending on the degree of visibility of neighbouring stations on the undulating surface of the ice sheet. The

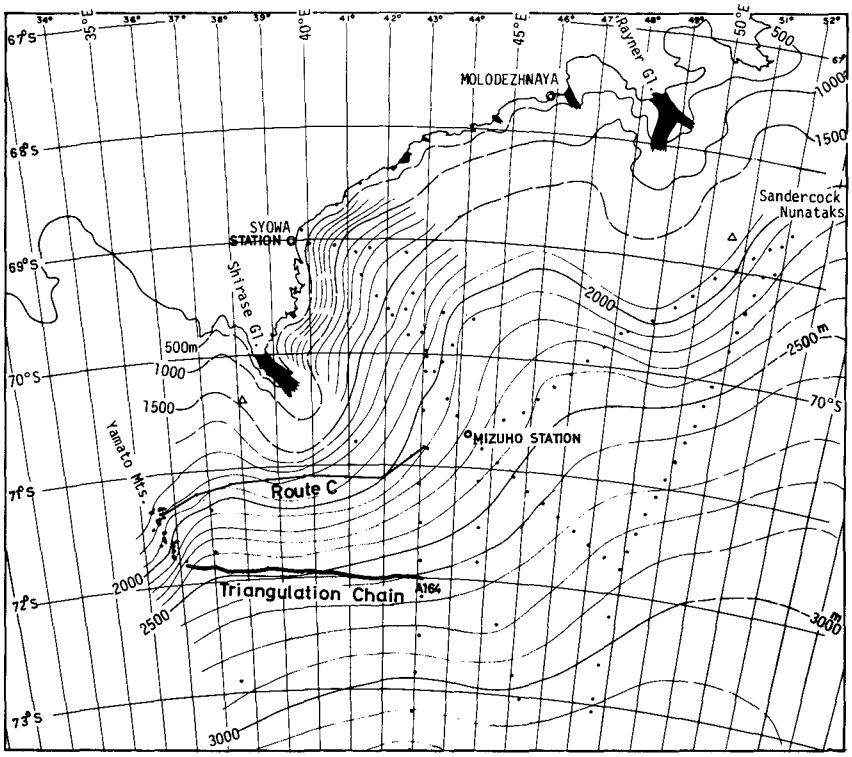

Fig. 1 A surface contour map of the ice sheet of Mizuho Plateau, East Antarctica. Dots indicate the principal stations along the Japanese oversnow traverse routes set up in 1968-1975. Surface contour lines are drawn at intervals of 100 m (after SHIMIZU *et al.* 1978a). A triangulation chain was installed along the parallel of 72°S from the southeast end of the Yamato Mountains to A164 (S240).

shortest side was 847.34 m of the base line, the longest 6379 m and the average 2966 m.

Each station was marked by the erection of a 3-m long metal pole or a 2.5-m long bamboo stake, both of which will be called a stake hereinafter. Twenty-two stakes out of 164 set up in 1969 were missing during the resurvey in 1973-1974. They must have been buried under heavy snow accumulations in the preceding four years. Additional 25 stations were set up to recover the continuity of the triangulation chain bringing the total number of surveying stations to 167 in the resurvey.

II. 2. *Procedure of survey*

Both the first and the second survey of the triangulation chain were conducted principally by angle measurements with Wild T2 theodolites. Measurements were made of the horizontal

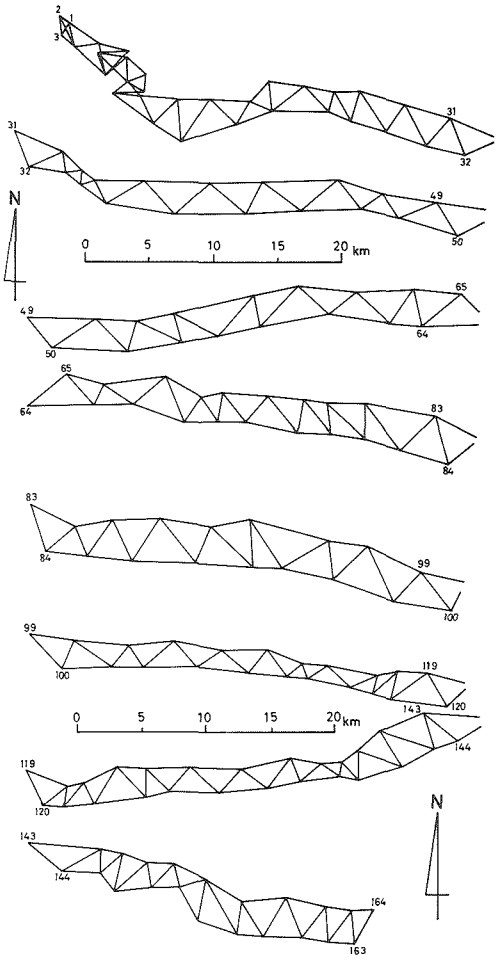

Fig. 2 Configuration of the triangulation chain from A001 to A164. Stations A001 and A002 were set up on the nunataks of the Yamato Mountains.

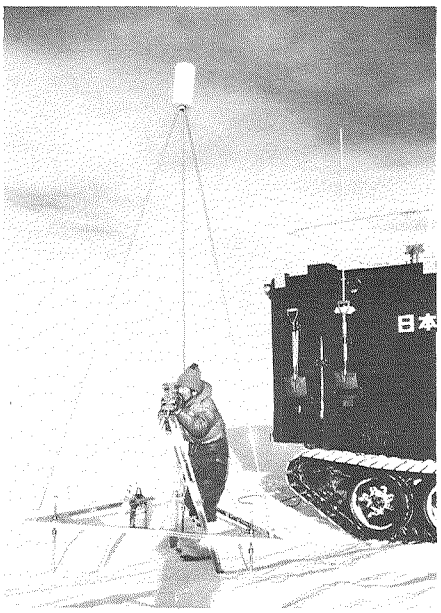

Fig. 3 Measurement of angles with a Wild T2 theodolite under a tripod target. A red-colour drum at the top of the tripod was used as a target for measurements.

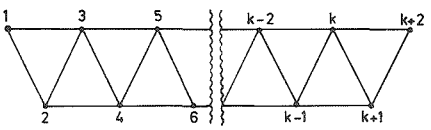

Fig. 4 A schematic figure of a part of the triangulation chain.

angles of the three interior angles of all the constituent triangles, and the vertical angles from each station to four neighbouring stations.

The field party was split into four groups, each with a theodolite and a tripod target which could be extended in height from 3.7 m to 4.7 m above the snow surface (see Fig. 3). The groups took charge of the stations in a manner of "leapfrogging", that is, the i-th group (i=1, 2, 3, 4) occupied the $(4k+i)$-th station successively (k=0, 1, 2,$\cdots$), (see Fig. 4), where the following operations were carried out :

(1) First survey (1969)
  a) Selecting a station at the optimum location.
  b) Setting a tripod target and measuring its height.
  c) Plumbing a point on the snow surface from the center of the target.
  d) Setting a theodolite exactly on the center point and measuring its height.
  e) Measuring the horizontal and vertical angles of the targets of four neighbouring stations.
  f) Setting a stake (also used as a snow stake) exactly at the center point and measuring its height.

(2) Second survey (1973-1974)
  a) Finding the stake and measuring its height.
  b) Setting a target exactly on the stake and measuring its height.
  c) Setting a theodolite as before and measuring its height.
  d) Measuring the angles as before.

The accuracy of angle measurement was nearly the same that is required by the standard operating procedure for the fourth order triangulation used in Japan ; namely, the limits of error allowed in angle measurements are 15 seconds as an observed differential, 25 seconds as a double angle difference, 20 seconds as a vertical angle constant difference, and 20 seconds as a closure error of a triangle. When a measured value showed an error beyond any of the above limitations, a remeasurement was made immediately. The number of days when observations were impossible due to heavy snow driftings was 10 out of 37 days in the first survey and 7 out of 28 days in the second survey. Measurements were also made of barometric elevation and surface slope at every station, and of ice thickness and gravity at optional stations.

II. 3. *Measurement of distance*

With the aim of correcting the accumulation of errors, the distance was measured with a radiowave distance meter (Cubic DM-20) and the azimuth was observed by shooting the sun for one side of every 10 to 15 triangles. The distance measurements were made two times for a side ; the difference between the two values of distance was in most cases found smaller than $0.02+5\times10^{-6}D_m$ (m), where D_m (m) was mean of the two values of distance. The distance calculated also by the chain using the angles measured was checked *in situ* against the distance measured by the meter.

The distance measured by the radiowave distance meter was subjected first to air temperature and pressure corrections to give the true distance D_m between the two instruments. Correction was not made for vapour pressure in the atmosphere, since the amount of water vapour is extremely small and its effect is negligible under a low temperature condition. Slope correction was secondly made with respect to the vertical angle so that the horizontal distance D_h between stations 1 and 2 could be obtained by

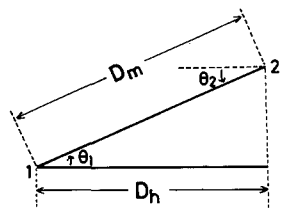

Fig. 5 Slope correction for measured distance D_m. Horizontal distance D_h can be obtained from values of θ_1, θ_2 and D_m.

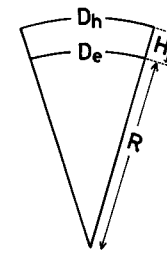

Fig. 6 Sea-level correction for horizontal distance D_h. Distance D_e on the sea level can be obtained from values of D_h, H and R.

$$D_h = D_m \cos \tfrac{1}{2}(\theta_1 - \theta_2), \tag{1}$$

where θ_1 is the vertical angle from station 1 to station 2 and θ_2 is that from station 2 to station 1. The sign of both θ_1 and θ_2 was positive upward and negative downward. A schematic figure of slope correction is shown in Fig. 5.

The horizontal distance D_h was subjected thirdly to sea-level correction, as shown in Fig. 6, that is,

$$D_e = D_h(1 - H/R), \tag{2}$$

where D_e is the distance on the sea level, H the mean elevation above the sea level of the two stations, and R the radius of curvature of the earth. The rough value of elevation measured by the barometric method was employed for H. The value of D_e was used as the observed distance in the computation of position, as described in the next sub-section.

II. 4. *Computation of position*

Positions, i.e., latitudes and longitudes, of all triangulation stations both in 1969 and 1973-1974 were calculated respectively by the observed data in each period by means of net-adjustment on the basis of the computer program developed by HARADA (1966). The principle of the net-adjustment is to calculate every position of a station in a geodetic chain or net by applying the least squares method to observation equations.

The triangulation chain was divided into three parts, namely A001-A049, A048-A117 and A116-A164. Computations of net-adjustment were made separately in each part. In the first part, positions of A001 and A002 were fixed as known ones ; positions of the other stations were unknown. Next, positions of A048 and A049 obtained in the first part, and those of A116 and A117 obtained in the second part were fixed as known ones respectively in the second and third

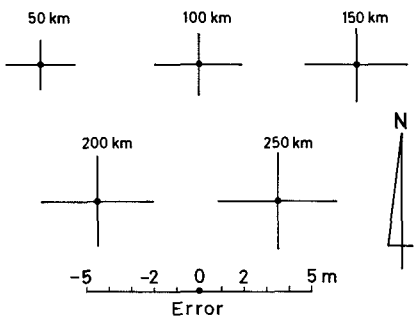

Fig. 7 Mean square errors (standard errors) of position at every 50 km from the datum point (A001) in the first survey (1969).

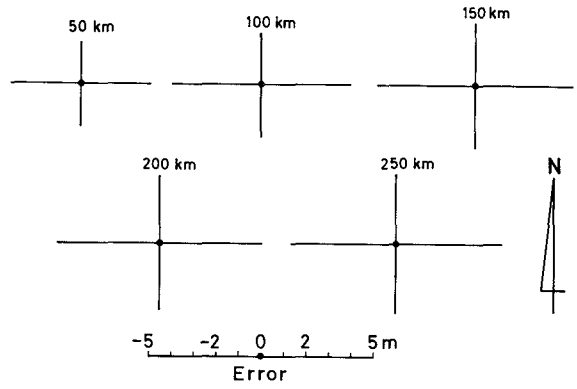

Fig. 8 Mean square errors (standard errors) of position at every 50 km from the datum point (A001) in the second survey (1973-1974).

parts, whereas positions of all the other stations of each part were unknown. One observation equation was constructed for each observation. Input data to an observation equation are approximate coordinates of stations with unknown positions, and both assumed and observed values of angle, azimuth or distance, while the unknown factors of the equation are correction terms to the approximate coordinates. By means of the least squares method applied to 510 observation equations, the most probable values of geodetic coordinates of all the stations of the chain were calculated. A reference ellipsoid used in the calculation was Bessel's ellipsoid ; namely, the radius of the equator is 6377397 m and the flattening ratio of the earth is 1/299.15.

As the results of the net-adjustment, the mean square errors (standard errors) of the geodetic coordinates were also obtained at all the triangulation stations, as illustrated in Fig. 7 (first survey) and Fig. 8 (second survey) at every 50 km from the datum point (A001). It is noted that the error increased gradually from the nearest 50 km towards the furthest end of the chain. The maximum errors resulted in the first survey were ± 2.14 m in latitude and ± 2.67 m in longitude at A164, and in the second survey ± 3.08 m in latitude and ± 4.70 m in longitude at A164, which were slightly larger.

II. 5. *Computation of elevation*

The horizontal distances of all the sides of the chain were calculated using the geodetic coordinates of the neighbouring stations obtained from the above net-adjustment.

The difference of elevation, Δh_{jk}, between stations j and k was then calculated by the following equation, as illustrated by a schema in Fig. 9 :

$$\Delta h_{jk} = \frac{1}{2} D_h (\tan\theta_1 - \tan\theta_2) + \frac{1}{2}(i_1 + f_1) - \frac{1}{2}(i_2 + f_2), \tag{3}$$

where D_h is the horizontal distance between stations j and k ; θ_1 and θ_2 are the vertical angles

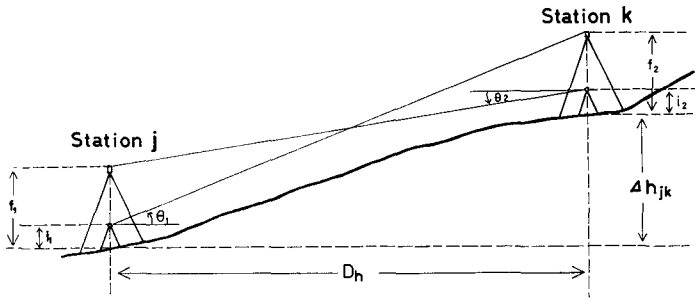

Fig. 9 A schema illustrating the method of measurement of vertical angles θ_1 and θ_2 from both Stations j and k to each other. Elevation difference Δh_{jk} can be calculated geometrically using values of θ, i, f and D_h.

from stations j and k ; i_1 and f_1 are the heights of the instrument and the target at station j respectively, their counterparts at station k being i_2 and f_2. Possible errors resulting from refraction due to the vertical gradient of air temperature and from the curvature of the earth can be counterbalanced, because measurements of vertical angles were carried out two times from both the stations in the opposite direction to one another and they were averaged, as shown in eq. (3).

The elevation H_k above the mean sea level of the k-th triangulation station was obtained by accumulating the elevation differences Δh successively onto elevation of a preceding station, as follows (see Fig. 4) :

$$H_2=H_1+\Delta h_{1\cdot 2},$$

and

$$H_k=\tfrac{1}{2}(H_{k-2}+\Delta h_{(k-2)k}+H_{k-1}+\Delta h_{(k-1)k}),\quad k\geq 3, \tag{4}$$

where H_1 was taken as 2254 m.

The mean square error in surface elevation was estimated at each triangulation station by applying the theory of propagation of error to eq. (4). The error increased gradually with an increase in the distance from the datum point. The tendency of accumulation of errors was almost the same between the first survey in 1969 and the second survey in 1973-1974. The maximum errors obtained were ± 0.88 m in the first survey and ± 0.84 m in the second survey at A164, the east end of the chain, which had the elevation of 354 m relative to the elevation of A001 (=0.0 m).

III. Calculation of flow vector and strain

III. 1. *Horizontal component of surface velocity*

The horizontal vector of ice movement was calculated at each triangulation station from the difference between two geodetic positions in 1969 and 1973-1974 which were obtained by net-adjustment. The horizontal displacement ΔS and its direction β indicated by the azimuth clockwise from the north point are given as follows :

$$\Delta S=\sqrt{(p\Delta\phi)^2+(q\Delta\lambda)^2}, \tag{5}$$

$$\beta=\tan^{-1}(q\Delta\lambda/p\Delta\phi), \tag{6}$$

where $\Delta\phi$ and $\Delta\lambda$ are respectively the difference of the latitudes and that of longitudes of a station between two measurements in 1969 and 1973-1974, and p and q are the coefficients of the reference ellipsoid (p is almost constant and q varies with the latitude of the station).

The horizontal component of the surface velocity V_h (m a^{-1}) is given by

$$V_h=\Delta S\cdot 365/N, \tag{7}$$

where N is the number of days between two observations ($1453\leq N\leq 1514$ days). Calculated values of V_h (m a^{-1}) and β (degree) are tabulated in Table 1 at a total of 140 stations. Also shown in Table 1 are each station's latitude, longitude, elevation, ice thickness (see Sub-section V. 3.), annual net accumulation (see Sub-section VI. 1.) and surface slope (see Sub-section V. 1.). The horizontal velocities V_h do not refer to the surface of the ice sheet, but to the surface of the reference ellipsoid. However, the difference of the two velocities is small ; for example, the value of 20 m a^{-1} on the ellipsoid corresponds to 20.008 m a^{-1} on the surface of the ice sheet 2500 m in elevation.

Mean square errors (standard errors) included in the displacement ΔS and azimuth β can be calculated from errors in $\Delta\phi$ and $\Delta\lambda$, by applying the theory of propagation of error to eqs. (5) and (6). An error in the velocity V_h is then obtained by dividing an error in ΔS by the number of elapsed years, i. e., $N/365$. Calculated errors at every ten stations along the chain are shown in Table 1. Since the surface flow is almost in a direction from south to north, the error in horizontal velocity was strongly controlled by the error included in latitude. The absolute value of error in V_h showed a gradual increase from the datum point towards the end of the chain (A164) ; the relative error showed the minimum value of 3 % at the middle part of the chain and 3 to 10 % in other parts. Errors in azimuth are given as large values at places where the displacement ΔS is small or the error in longitude is large. As the result, the absolute value of error in β showed the minimum value of 3 degrees at the middle part of the chain and 3 to 6 degrees in other parts.

Table 1. Three components of the surface velocity (namely V_h, β, V_z) and morphological data at 140 stations of the triangulation chain.

(Notes)

Latitude and longitude: Geodetic position of each station in December 1973 – January 1974 (N 1975).

Elevation: Elevation (a.s.l.) of each station in 1973-1974 (NARUSE and YOKOYAMA 1975).

Ice thickness: Data with and without the asterisk are respectively from SHIMIZU et al. (1972) and NARUSE and YOKOYAMA (1975). Thicknesses which show large discrepancies with the distribution of gravity values (YOSHIDA and YOSHIMURA 1972) are eliminated from the table.

Error: Mean square error (standard error) calculated at every 10 stations.

Azimuth of velocity: Direction of the horizontal flow measured clockwise from north.

Emergence (submergence) velocity: Positive and negative values show emergence and submergence velocities respectively.

Net accumulation: Mean annual net accumulation in m of snow depth (YOKOYAMA 1975).

Surface slope: Surface slope along the ice flow direction reduced from skyline measurements (NARUSE 1975).

Station	Latitude (S)	Longitude (E)	Elevation (m)	Ice Thickness (m)	Horizontal Velocity (m a^{-1})		Azimuth of Velocity (degree)		Emergence (Submergence) Velocity (m a^{-1})		Net Accumulation (m a^{-1})	Surface Slope (min)
					V_h	error	β	error	V_z	error		
A003	71°48′03″	36°11′17″	2250	* 436	0.22		335		+0.03		−0.06	60
004	71 48 34	36 13 07	2269	* 595	0.33		342		+0.02			40
005	71 48 24	36 16 13	2281		0.40	±0.03	342	±6.2	+0.09	±0.04	−0.05	45
006	71 49 46	36 17 14	2318		0.75		333		+0.08		−0.07	40
007	71 48 44	36 20 14	2294		0.64		329		+0.06		−0.02	40
008	71 48 47	36 16 09	2286	* 556	0.45		339		+0.04		−0.07	30
009	71 48 57	36 19 54	2296		0.65		327		+0.06			40
010	71 50 00	36 19 56	2338	* 390	0.78		323		+0.05		−0.07	35
011	71 49 43	36 22 31	2334		1.03		327		+0.04		−0.04	50
012	71 50 26	36 22 11	2351		0.99		314		+0.05		−0.06	40
013	71 50 28	36 17 56	2336		0.87		314				−0.05	40
014	71 50 36	36 21 55	2351	* 590	0.90		309		+0.04		+0.05	35
015	71 51 45	36 23 18	2353		1.1	±0.11	313	±5.8	+0.07	±0.06	−0.05	40
016	71 50 47	36 26 43	2370	* 923	1.1		319		+0.07			0
017	71 52 34	36 26 59	2376		1.5		322		+0.08		−0.04	50
018	71 50 48	36 30 59	2377	*1094	1.8		332		+0.07		−0.05	25
019	71 51 52	36 34 28	2387		2.1		338		+0.01		+0.03	20
020	71 50 53	36 36 25	2388	1692	3.6		348		+0.01		−0.04	30
021	71 51 18	36 39 18	2391		3.7		345		+0.02		−0.01	15
022	71 50 05	36 38 55	2375	1692	4.6		349		+0.01		−0.04	25
023	71 50 16	36 43 44			4.1		348				−0.01	13
024	71 51 20	36 47 01	2382		4.1		346		−0.06	±0.09	−0.04	42
025	71 50 31	36 47 42	2377	1440	4.1	±0.25	347	±5.2				26
026	71 51 45	36 50 00	2395		4.1		346		0		−0.03	36
027	71 50 32	36 51 05	2375	1485	4.3		343		−0.25		+0.14	24
028	71 52 10	36 54 40	2397		4.1		348		−0.19		+0.10	24
029	71 51 04	36 57 00	2394	1692	4.2		344		−0.03		−0.03	16

Station	Latitude	Longitude	Elevation	Ice Thickness	Horizontal Velocity (m a^{-1})		Azimuth of Velocity (degree)		Emergence (Submergence) Velocity (m a^{-1})		Net Accumulation	Surface Slope
	(S)	(E)	(m)	(m)	V_h	error	β	error	V_z	error	(m a^{-1})	(min)
A030	71°52′45″	36°59′55″	2414		4.1		353					16
031	71 51 35	37 03 00	2410	1620	3.8		357		−0.07		−0.05	14
032	71 53 05	37 04 56	2416		4.0		359		−0.21		+0.17	14
033	71 52 26	37 09 40	2411	1521	4.1		6		−0.23		+0.20	16
034	71 53 20	37 10 04	2425		4.2		7		−0.07		+0.13	18
035	71 53 12	37 12 08	2423	1557	4.5	±0.37	12	±6.4	−0.06	±0.11	−0.04	29
036	71 53 48	37 11 56	2433		4.3		12		−0.08		+0.06	16
037	71 53 36	37 13 54	2427	1800	4.7		15		−0.11		−0.04	16
038	71 54 34	37 15 18	2432		4.6		14		−0.24		+0.19	14
039	71 53 35	37 20 25	2419		5.6		16		−0.14		−0.03	18
040	71 54 57	37 24 21	2426		5.9		14		−0.33		+0.32	16
041	71 53 37	37 29 05	2412		7.1		14		−0.23		+0.23	13
042	71 54 50	37 33 56	2414		7.7		9		−0.28		+0.15	14
043	71 53 32	37 35 55	2405	1620	8.5		10		−0.24		+0.27	16
044	71 54 42	37 41 13	2412		8.5		7		−0.24		+0.25	17
045	71 53 23	37 46 02	2399	1809	9.0	±0.55	6	±5.4	−0.15	±0.13	+0.25	15
046	71 54 33	37 49 08	2409		8.6		4		−0.11		+0.16	14
047	71 53 56	37 51 58	2410		8.9		4		+0.06		−0.05	18
049	71 54 13	37 59 09	2412	1746	9.6		5		+0.10		−0.05	19
051	71 54 30	38 08 21	2415	1980	11.2		9		+0.07		+0.13	18
052	71 55 54	38 12 23	2426		12.2		10		−0.01		+0.07	22
053	71 54 41	38 13 49	2410	2052	13.3		11		−0.13		+0.14	21
054	71 55 40	38 19 32	2417		14.9		7		−0.14		+0.10	19
055	71 54 28	38 18 39	2404	1935	15.1	±0.64	9	±3.8	−0.13	±0.15	−0.04	22
056	71 55 28	38 24 21	2414		16.8		6		−0.15		+0.15	19
057	71 53 55	38 29 29	2398	1701	18.1		6		−0.04		−0.01	20
059	71 53 40	38 35 23	2392	1746	18.8		5		−0.13		+0.16	20
060	71 54 52	38 39 16	2404		18.5		3		−0.22		+0.19	20
061	71 54 01	38 43 06	2397	1800	19.2		4		−0.18		+0.04	19
062	71 55 21	38 47 24	2406		19.1		3		−0.13		+0.03	34
063	71 53 58	38 50 38	2387		19.8		3		−0.36		+0.15	26
064	71 55 31	38 51 31	2408		19.4		3		−0.22		−0.01	30
065	71 54 16	38 56 57	2382	1719	20.4	±0.67	1	±3.0	−0.71	±0.18	+0.22	30
066	71 55 33	39 00 39	2422		20.3		1		−0.57		−0.08	24
067	71 54 44	39 01 54	2401	1980	20.9		1		−0.67		−0.04	24
068	71 55 35	39 06 00	2421		20.5		1		−0.84		+0.20	22
069	71 54 28	39 10 19	2405	1989	21.3		0		−0.76		+0.04	24
070	71 56 21	39 12 38	2430		20.2		2		−0.82		+0.16	22
071	71 55 19	39 14 59	2416	1917	21.0		1		−0.78		+0.02	24
072	71 56 21	39 17 02	2429		20.4		2		−0.87		+0.13	21
073	71 55 11	39 17 46	2413	2178	21.0		1		−0.87		+0.14	21
075	71 55 18	39 23 45	2411	2160	20.7	±0.73	0	±3.2	−0.92	±0.20	+0.21	16
076	71 56 48	39 27 46	2425		19.8		0		−0.90		+0.28	16
077	71 55 28	39 28 29	2417	2097	20.3		359		−0.81		+0.20	17

Station	Latitude (S)	Longitude (E)	Elevation (m)	Ice Thickness (m)	Horizontal Velocity (m a^{-1}) V_h	error	Azimuth of Velocity (degree) β	error	Emergence (Submergence) Velocity (m a^{-1}) V_z	error	Net Accumulation (m a^{-1})	Surface Slope (min)
A078	71°56′51″	39°32′00″	2432		19.5		359		−0.78		+0.02	16
079	71 55 35	39 31 27	2422	2115	20.2		359		−0.77		−0.05	18
080	71 57 02	39 36 34	2439		19.4		359		−0.64		+0.01	20
081	71 55 35	39 36 28	2419	2142	20.1		359		−0.86		+0.14	22
082	71 57 26	39 41 19	2443		19.1		359		−0.73		+0.05	20
083	71 56 00	39 45 51	2429	2115	19.6		359		−0.87		+0.26	19
084	71 57 58	39 47 52	2447		18.8		359		−0.95		+0.25	19
085	71 56 55	39 51 54	2442	2070	19.3	±0.76	359	±3.5	−0.78	±0.22	0.00	15
086	71 58 11	39 53 33	2449		18.9		359		−0.89		+0.23	16
087	71 56 41	39 56 54	2434	2169	19.5		359		−1.00		+0.25	19
089	71 56 36	40 03 00	2426	2151	19.5		358		−1.11		+0.33	18
090	71 58 17	40 08 26	2444		19.1		356		−0.87		+0.05	23
092	71 58 13	40 15 55	2458		18.7		355		−0.82		−0.05	23
094	71 58 11	40 20 02	2455		18.4		355		−0.96		+0.11	27
095	71 56 54	40 25 53	2452	2070	18.5	±0.80	354	±3.7	−0.93	±0.23	−0.03	19
096	71 58 27	40 26 55	2465		17.8		355		−1.05		+0.36	17
097	71 57 01	40 31 01	2457		18.2		354		−1.06		+0.29	15
098	71 59 08	40 35 06	2478		17.3		355		−0.96		0.00	16
099	71 57 51	40 38 28	2466	2322	17.9		354		−1.07		+0.13	16
100	71 59 18	40 42 52	2482		17.3		354		−1.04		+0.21	18
101	71 58 06	40 44 25	2472	2160	17.8		353		−1.01		+0.07	19
102	71 59 14	40 49 26	2480		17.4		353		−1.10		+0.18	18
103	71 58 21	40 51 47	2476	2160	17.8		352		−0.97		+0.09	17
105	71 58 16	40 57 46	2482		17.5	±0.85	352	±3.9	−1.03	±0.25	+0.10	17
107	71 58 41	41 04 03	2485	2079	17.4		352		−1.11		+0.45	18
108	71 59 38	41 07 30	2495		17.1		351		−1.07		+0.10	18
109	71 58 41	41 10 02	2489	2061	17.4		351		−1.04		+0.20	18
110	71 59 50	41 12 32	2503		17.0		351		−1.00		+0.30	18
111	71 59 19	41 14 40	2502		17.1		351		−1.03		+0.18	17
112	71 59 56	41 15 04	2508		17.0		351		−1.11		+0.33	17
113	71 59 27	41 17 51	2501		16.9		351		−0.94		+0.10	17
114	72 00 23	41 20 37	2515		16.7		350		−0.91		+0.12	21
115	72 00 00	41 24 28	2510	2079	16.6	±0.91	350	±4.3	−1.02	±0.26	+0.13	25
116	72 00 44	41 23 28	2524		16.3		350		−0.85		+0.04	23
117	71 59 55	41 27 02	2515	2061	16.3		350		−1.19		+0.50	19
118	72 01 01	41 25 38	2531		16.1		350		−1.05		+0.30	16
120	72 01 28	41 33 12	2540		15.3		349		−0.86		+0.02	21
121	72 00 41	41 36 25	2533		15.3		349		−0.89		−0.01	26
122	72 01 32	41 35 56	2545		14.9		349		−0.94		+0.15	19
123	72 00 30	41 38 46	2533	1890	15.0		349		−0.90		+0.04	18
125	71 59 51	41 43 07	2536	2088	14.8	±0.92	349	±4.8	−0.78	±0.27	−0.01	18
126	72 01 05	41 46 56	2548		14.1		351		−1.01		+0.08	14
127	71 59 55	41 47 00	2539		14.6		350		−0.94		+0.14	19
128	72 00 51	41 50 03	2548		14.1		352		−1.03		+0.23	15

Station	Latitude	Longitude	Elevation	Ice Thickness	Horizontal Velocity (m a^{-1})		Azimuth of Velocity (degree)		Emergence (Submergence) Velocity (m a^{-1})		Net Accumulation	Surface Slope
	(S)	(E)	(m)	(m)	V_h	error	β	error	V_z	error	(m a^{-1})	(min)
A129	71°59′50″	41°52′59″	2535		14.4		351		−1.00		+0.10	18
130	72 00 54	41 56 54	2541		14.0		352		−1.08		+0.32	14
131	71 59 55	41 59 57	2534		14.2		351		−0.81		+0.07	14
133	71 59 30	42 06 26	2529	2250	14.4		349		−1.10		+0.47	13
135	71 59 43	42 10 34	2524	2178	14.4	±0.94	348	±5.1	−1.08	±0.28	+0.40	13
138	72 00 27	42 15 24	2514		14.4		346		−0.91		+0.17	12
140	71 59 57	42 21 21	2534		14.8		343		−0.92		−0.03	31
141	71 58 27	42 18 27	2516		14.7		344		−1.02		+0.57	7
142	71 59 14	42 25 39	2548		14.8		343		−0.93		0.00	25
144	71 58 55	42 28 38	2550		14.7		343		−0.78		+0.14	24
145	71 57 59	42 33 56	2541	2070	14.7	±0.97	343	±5.0	−0.82	±0.29	+0.10	25
146	71 58 56	42 33 51	2559		14.5		344		−0.75		+0.11	20
147	71 58 06	42 36 52	2550		14.5		343					20
148	71 59 40	42 35 42	2568		14.1		345		−0.94		+0.16	15
149	71 58 28	42 39 55	2556		14.2		344		−0.90		+0.17	16
151	71 58 28	42 43 32	2551		14.1		344		−0.76		+0.14	13
154	72 00 50	42 46 34	2577		13.7		343					18
155	72 01 24	42 52 04	2588		13.3	±0.99	341	±5.5	−0.77	±0.30	−0.04	16
157	72 01 27	42 55 20	2584		13.3		338					19
159	72 01 26	43 00 30	2601		13.4		336		−0.71		−0.03	20
160	72 00 08	43 03 33	2581	2349	13.7		335		−0.69		+0.18	24
161	72 01 32	43 03 55	2614		13.3		336		−0.64		−0.01	21
162	72 00 12	43 06 58	2600		13.6		336		−0.64		−0.02	16
163	72 01 32	43 07 27	2619		13.3		336		−0.70		+0.01	18
164	72 00 07	43 09 48	2606		13.6	±1.01	336	±5.2	−0.64	±0.31	+0.06	12

III. 2. *Emergence or submergence velocity*

The surface elevations of the ice sheet in 1969 and 1973-1974 were calculated by eq. (4) at each surveying station along the chain. The vertical displacement ΔH of the top of a stake was obtained by subtracting the thickness of net accumulation of snow for a period of four years from the difference of the above two surface elevations.

Now, we obtain the "emergence or submergence velocity" V_z of the surface flow. Figure 10 shows schematically the movement of a stake from 1969 to 1973-1974 in the accumulation area with a submergence flow. The horizontal displacement ΔS (m) and the vertical displacement ΔH (m) of the top of the stake are measured with respect to the coordinate fixed on the bedrock, and the sign of ΔH is taken positive upward in this paper. The horizontal component of the flow velocity V_h (m a^{-1}) is $\Delta S \cdot 365/N$, where N is the number of days between two observations. Should an ice flow be parallel to the surface, ΔH would be equal to $-\Delta S \tan\theta_s$, where θ_s is the surface slope (positive sign) along the flow direction. But the ice

flow is in this case downward relative to the surface, so the absolute value of the vertical displacement ΔH is larger than $\Delta S \tan\theta_s$ by an amount of $V_z \cdot N/365$ (m); namely,

$$-\Delta H=\Delta S \tan\theta_s - V_z \cdot N/365,$$

then

$$V_z=(\Delta H+\Delta S\tan\theta_s)\,365/N= V_z'+ V_h \tan\theta_s, \tag{8}$$

where V_z' is the vertical velocity component (positive upward) of the top of the stake, that is $\Delta H \cdot 365/N$. Then, the positive value of V_z indicates emergence velocity and the negative value of V_z indicates submergence velocity at the ice sheet surface. The mean square error (standard error) included in V_z was calculated at each station from the errors in ΔH, ΔS and θ_s which was assumed as ± 10 min. (1/350). The values of V_z at all the stations and the errors at every ten stations are also shown in Table 1. Relative errors in the emergence or submergence velocity were considerably large in the region from A003 to around A060 where V_z was very small, while in the region eastward from A060 relative errors showed rather small values in a range from 22 % to 48 %. The component V_p perpendicular to the ice sheet surface is obtained as $V_p= V_z \cos\theta_s$. However, since the value of the surface slope was smaller than one degree all over the area along the triangulation chain, V_p is regarded as equal to V_z in this paper.

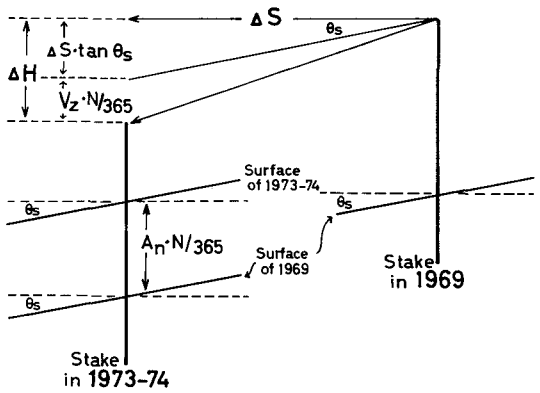

Fig. 10 A schematic figure showing the movement of a stake in the period from 1969 to 1973-1974.
ΔS: Horizontal displacement during the period,
ΔH: Vertical displacement during the period,
V_z: Emergence or submergence velocity per year,
A_n: Annual net accumulation in the thickness of snow,
θ_s: Surface slope (positive sign) along the ice flow direction,
N: Number of days between two observations.
The signs of ΔH, V_z and A_n are taken positive upward. The diagram refers to the region of the "submergence flow".

III. 3. *Strain rate of the ice sheet surface*

Square strain grids approximately 1 km in each side were installed and surveyed separately at nine stations over Mizuho Plateau in 1969-1970 (NARUSE *et al.* 1972), seven of which were resurveyed during the period from 1970 to 1975 (SATOW 1977). Two types of square strain grids were actually set up : the four-stake grid and the five-stake grid. The former had a stake

at each corner of a square with a side approximately 1 km long, whereas the latter had an additional stake at the intersection of two diagonals, as illustrated in Fig. 11. The length of one diagonal was measured with a radiowave distance meter (Cubic DM-20) and each interior angle of the constituent triangles with Wild T2 theodolites. Methods of observations and data corrections are the same as those of the triangulation chain mentioned in the foregoing section.

The check of the homogeneity of strain in the area approximately 1 $(km)^2$ was made by examining the standard deviation of strain rate among the four values obtained from the respective four triangles of a five-stake grid. Principal strain rates $\dot{\varepsilon}_1$ and $\dot{\varepsilon}_2$ at Mizuho Station (70°42'S ; 44°20'E) were given as

$$\dot{\varepsilon}_1=(+0.9\pm0.11)\times10^{-4} \qquad (a^{-1})$$

and

$$\dot{\varepsilon}_2=(-4.0\pm0.12)\times10^{-4} \qquad (a^{-1}).$$

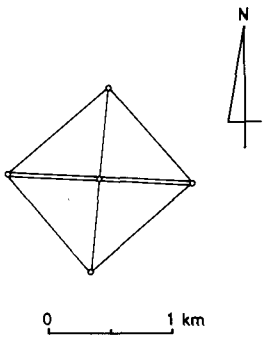

Fig. 11 Configuration of a five-stake strain grid at Mizuho Station. Distance measurement was made of a diagonal shown by a double line ; angle measurement was made of every interior angle.

Since the deviations are small compared with the mean strain rates, it is considered that the homogeneous strain on the scale of 1 km holds approximately in the area around Mizuho Station.

The surface deformation of the ice sheet was consequently calculated on each triangle of the triangulation chain, assuming that the strain was homogeneous on the scale of individual triangles in this survey. The method of calculation of strain rate was to get the rate of transformation of a circumscribed circle about a triangle into an ellipse caused by a homogeneous strain (JAEGER 1969). Geodetic coordinates of three points of each triangle were obtained both in 1969 and 1973-1974, by the net-adjustment of the chain. If the amount of the translation is subtracted from the displacement of a triangle, the pure strain and rotation of the ice sheet surface can be calculated : the former specifies the shape of the strain ellipse, while the latter gives the rotation of the principal axes of the strain. Taking a radius of the circumscribed circle about an initial triangle as unity, and lengths of major and minor axes of the strain ellipse as $2F$ and $2G$, the parameters of the ice deformation can be represented as the function of F and G. As the results of calculations to determine the values of F and G from the coordinates of the points of a triangle concerned, the following strain rate parameters were obtained at 140 triangles of the chain :

α: Direction of the principal axis of the strain ε_1 (see below), indicated by the azimuth from north.

Table 2. Strain parameters of the ice sheet surface at each triangle of the triangulation chain.
Explanations of the symbols are given in the text. (after NARUSE 1978).

Triangle	α (degree)	$\dot{\varepsilon}_1$ $\times 10^{-4}$ (a^{-1})	$\dot{\varepsilon}_2$ $\times 10^{-4}$ (a^{-1})	$\dot{\Delta}$ $\times 10^{-4}$ (a^{-1})	$\dot{\gamma}_{max}$ $\times 10^{-4}$ (a^{-1})	$\dot{\omega}$ (° a^{-1})
1. 2. 3	97.34	+0.46	−1.49	−1.02	1.95	+0.005
1. 2. 4	100.54	+0.51	−2.15	−1.64	2.66	+0.006
1. 3. 4	86.45	+0.50	−1.70	−1.20	2.20	+0.003
1. 4. 5	71.00	−0.03	−1.63	−1.66	1.60	0
2. 3. 4	81.85	+0.48	−1.39	−0.92	1.87	+0.002
4. 5. 6	61.28	+0.09	−1.39	−1.30	1.48	+0.001
5. 6. 7	54.33	−0.28	−1.46	−1.74	1.17	+0.001
6. 7. 8	54.76	−0.27	−1.64	−1.91	1.38	0
6. 8. 9	56.52	−0.43	−1.61	−2.04	1.18	+0.001
6. 10. 13	34.60	+1.10	−0.93	+0.17	2.04	+0.006
8. 9. 10	35.62	−0.03	−1.20	−1.23	1.17	0
9. 10. 11	40.64	+0.58	−1.76	−1.18	2.34	−0.003
10. 11. 12	24.40	+1.69	−1.57	+0.17	3.26	0
10. 12. 13	42.84	+0.97	−1.59	−0.62	2.57	+0.006
10. 13. 14	36.78	+1.04	−0.80	+0.24	1.84	+0.006
11. 14. 16	26.37	+2.08	−0.53	+1.55	2.62	−0.001
13. 14. 15	86.08	−0.31	−1.00	−1.31	0.69	+0.002
14. 15. 16	53.96	+0.45	−1.05	−0.59	1.50	−0.001
15. 16. 17	55.65	+0.48	−1.73	−1.25	2.21	−0.002
16. 17. 18	49.51	+1.10	−2.45	−1.36	3.55	−0.006
17. 18. 19	52.22	+1.03	−0.70	+0.33	1.73	−0.004
18. 19. 20	27.80	+6.56	−1.36	+5.19	7.91	−0.018
18. 20. 22	42.53	+3.15	−2.09	+1.05	5.24	−0.021
19. 20. 21	16.00	+7.16	−1.81	+5.34	8.96	−0.008
20. 21. 22	15.29	+4.65	−1.77	+2.88	6.41	−0.006
21. 22. 23	174.81	+3.82	+0.02	+3.85	3.80	+0.006
21. 23. 24	29.79	+1.37	−0.48	+0.89	1.84	0
23. 24. 25	42.06	+0.44	−0.33	+0.10	0.77	+0.003
24. 25. 26	62.01	+0.77	−0.14	+0.62	0.91	+0.002
25. 26. 27	177.14	+0.35	−1.98	−1.63	2.33	−0.004
26. 27. 28	144.56	+0.78	−0.32	+0.46	1.10	−0.005
27. 28. 29	142.49	+0.78	−0.63	+0.16	1.41	−0.004
28. 29. 30	127.90	+1.31	−0.49	+0.82	1.80	−0.006
29. 30. 31	104.08	+2.90	−0.55	+2.35	3.45	0
30. 31. 32	88.58	+1.37	−0.88	+0.49	2.25	+0.001
31. 32. 33	81.43	+1.75	−0.74	+1.02	2.49	0
32. 33. 34	88.64	+1.98	−0.77	+1.21	2.76	−0.002

Table 2(−2)

Triangle	α (degree)	$\dot{\varepsilon}_1$ $\times 10^{-4}$ (a^{-1})	$\dot{\varepsilon}_2$ $\times 10^{-4}$ (a^{-1})	$\dot{\Delta}$ $\times 10^{-4}$ (a^{-1})	$\dot{\gamma}_{max}$ $\times 10^{-4}$ (a^{-1})	$\dot{\omega}$ (°a^{-1})
33 . 34 . 35	77.78	+4.03	−0.76	+3.26	4.79	−0.006
34 . 35 . 36	74.67	+4.04	+0.97	+5.02	3.07	−0.005
35 . 36 . 37	61.07	+3.18	+0.51	+3.68	2.67	−0.006
36 . 37 . 38	51.48	+3.50	+0.03	+3.53	3.46	−0.002
37 . 38 . 39	40.07	+2.70	−0.32	+2.37	3.02	−0.004
38 . 39 . 40	42.46	+2.66	−0.86	+1.79	3.52	−0.004
39 . 40 . 41	36.04	+2.79	−0.99	+1.80	3.79	−0.007
40 . 41 . 42	37.25	+2.81	−2.47	+0.34	5.28	−0.006
41 . 42 . 43	37.25	+3.06	−2.46	+0.59	5.52	−0.006
42 . 43 . 44	27.67	+2.84	−1.08	+1.75	3.92	0
43 . 44 . 45	19.62	+1.56	−1.22	+0.35	2.78	−0.001
44 . 45 . 46	8.21	+2.36	−1.10	+1.26	3.46	+0.002
45 . 46 . 47	14.57	+2.47	−0.58	+1.89	3.05	+0.003
46 . 47 . 49	55.06	+1.19	−0.70	+0.49	1.89	−0.005
49 . 51 . 52	71.92	+1.81	−2.15	−0.34	3.96	−0.008
51 . 52 . 53	48.51	+6.17	−1.52	+4.64	7.69	−0.016
52 . 53 . 54	36.99	+5.19	−3.78	+1.40	8.97	−0.012
53 . 54 . 55	33.94	+5.03	−3.68	+1.35	8.71	−0.015
54 . 55 . 56	35.40	+5.24	−3.42	+1.81	8.66	−0.015
55 . 56 . 57	44.39	+2.41	−3.74	−1.33	6.15	−0.011
56 . 57 . 60	19.10	+3.40	−1.47	+1.92	4.87	−0.001
57 . 59 . 60	21.56	+3.37	−1.37	+2.00	4.74	0
59 . 60 . 61	22.92	+3.02	−1.22	+1.80	4.23	+0.002
60 . 61 . 62	28.14	+2.55	−0.96	+1.59	3.50	−0.001
61 . 62 . 63	22.13	+2.10	−1.15	+0.94	3.24	−0.002
62 . 63 . 64	25.65	+1.98	−0.29	+1.69	2.27	−0.004
63 . 64 . 65	17.02	+1.92	−1.53	+0.39	3.45	−0.006
64 . 65 . 66	8.32	+2.17	−0.76	+1.42	2.93	−0.007
65 . 66 . 67	10.16	+2.88	−1.03	+1.85	3.92	−0.010
66 . 67 . 68	175.46	+3.49	−0.06	+3.43	3.55	−0.007
67 . 68 . 69	173.62	+3.07	+0.05	+3.12	3.02	−0.005
68 . 69 . 70	171.13	+3.35	+0.11	+3.46	3.24	−0.005
69 . 70 . 71	175.65	+3.44	+0.66	+4.10	2.78	−0.006
70 . 71 . 72	172.70	+3.63	+0.74	+4.37	2.89	−0.005
71 . 72 . 73	162.52	+3.32	+0.33	+3.65	2.99	−0.003
72 . 73 . 75	169.74	+3.28	−1.63	+1.65	4.92	−0.001
72 . 75 . 76	171.56	+2.79	−1.77	+1.01	4.56	−0.001
75 . 76 . 77	169.77	+2.40	−1.10	+1.31	3.50	+0.002
76 . 77 . 78	168.62	+2.41	−0.82	+1.59	3.22	+0.002

Table 2(−3)

Triangle	α (degree)	$\dot{\varepsilon}_1$ $\times 10^{-4}$ (a^{-1})	$\dot{\varepsilon}_2$ $\times 10^{-4}$ (a^{-1})	$\dot{\Delta}$ $\times 10^{-4}$ (a^{-1})	$\dot{\gamma}_{max}$ $\times 10^{-4}$ (a^{-1})	$\dot{\omega}$ (° a^{-1})
77. 78. 79	178.26	+2.74	−0.05	+2.68	2.79	+0.002
78. 79. 80	0.70	+2.76	+0.07	+2.84	2.69	+0.001
79. 80. 81	177.92	+2.42	+0.16	+2.57	2.26	+0.002
80. 81. 82	177.58	+2.42	+0.65	+3.06	1.77	+0.002
81. 82. 83	173.69	+2.52	+0.02	+2.54	2.50	+0.001
82. 83. 84	175.18	+2.25	+0.10	+2.35	2.14	0
83. 84. 85	177.96	+2.30	+0.11	+2.41	2.18	−0.001
84. 85. 86	10.77	+1.80	−0.35	+1.45	2.15	−0.001
85. 86. 87	12.47	+1.85	−0.27	+1.58	2.12	−0.001
86. 87. 89	9.05	+2.25	−1.48	+0.76	3.73	+0.003
86. 89. 90	4.55	+1.76	−1.00	+0.76	2.76	0
89. 90. 92	166.40	+0.68	−1.22	−0.54	1.89	+0.003
92. 94. 95	153.47	+2.99	−0.60	+2.39	3.58	−0.001
94. 95. 96	151.46	+2.86	−0.56	+2.29	3.41	−0.001
95. 96. 97	151.13	+2.83	−0.21	+2.62	3.04	−0.002
96. 97. 98	161.44	+1.99	−0.48	+1.51	2.48	−0.001
97. 98. 99	170.35	+2.23	−0.42	+1.80	2.65	−0.004
98. 99.100	171.20	+2.35	−0.60	+1.75	2.95	−0.003
99.100.101	171.46	+2.33	−0.50	+1.82	2.83	−0.002
100.101.102	174.23	+2.25	−0.75	+1.49	3.00	−0.002
101.102.103	175.74	+2.06	−0.62	+1.45	2.68	−0.001
102.103.105	163.66	+2.99	−0.24	+2.76	3.22	0
105.107.108	8.23	+1.28	−0.06	+1.22	1.34	+0.002
107.108.109	4.02	+1.52	−0.35	+1.17	1.86	+0.001
108.109.110	0.25	+1.62	−0.22	+1.40	1.84	+0.001
109.110.111	176.12	+1.41	−0.08	+1.34	1.49	+0.002
110.111.112	179.50	+1.27	−0.13	+1.14	1.40	+0.002
111.112.113	168.99	+1.22	−0.31	+0.91	1.53	+0.003
112.113.114	179.08	+0.93	−0.48	+0.45	1.41	+0.004
113.114.115	9.48	+0.84	0.00	+0.83	0.84	+0.006
114.115.116	160.89	+2.44	+0.18	+2.62	2.26	+0.003
115.116.117	160.44	+2.86	−0.30	+2.56	3.16	+0.006
116.117.118	153.69	+1.97	−0.10	+1.87	2.07	+0.003
117.118.120	161.04	+1.84	−0.55	+1.29	2.39	+0.004
117.120.121	160.47	+1.66	−0.30	+1.36	1.97	+0.005
120.121.122	142.18	+3.78	−0.09	+3.69	3.87	+0.002
121.122.123	142.96	+4.00	−0.39	+3.61	4.38	+0.004
123.125.126	137.44	+2.58	−0.11	+2.47	2.68	−0.001
125.126.127	141.28	+2.59	+0.72	+3.31	1.87	−0.001

Table 2(−4)

Triangle	α (degree)	$\dot{\varepsilon}_1$ $\times 10^{-4}$ (a^{-1})	$\dot{\varepsilon}_2$ $\times 10^{-4}$ (a^{-1})	$\dot{\Delta}$ $\times 10^{-4}$ (a^{-1})	$\dot{\gamma}_{max}$ $\times 10^{-4}$ (a^{-1})	$\dot{\omega}$ (°a^{-1})
126.127.128	149.24	+2.30	+0.58	+2.88	1.72	−0.002
127.128.129	151.13	+2.38	0.00	+2.38	2.38	−0.003
128.129.130	158.91	+1.95	−0.19	+1.76	2.13	−0.003
129.130.131	155.17	+1.86	−0.41	+1.45	2.28	−0.002
130.131.133	171.51	+1.06	−0.81	+0.25	1.88	−0.002
130.133.138	9.05	+0.86	−1.45	−0.59	2.32	+0.001
133.138.141	173.59	+0.46	−1.80	−1.33	2.26	−0.001
138.140.141	0.55	+0.27	−2.18	−1.91	2.45	−0.002
140.141.142	19.43	+0.25	−0.85	−0.59	1.10	+0.002
141.142.144	141.32	+0.44	−1.34	−0.91	1.78	+0.006
141.144.145	125.04	+0.06	−0.74	−0.69	0.80	+0.003
144.145.146	128.10	+2.05	−0.45	+1.60	2.49	−0.004
145.146.147	131.27	+1.72	−0.46	+1.27	2.18	−0.004
146.147.148	136.60	+2.62	−0.42	+2.20	3.05	−0.003
147.148.149	137.73	+2.36	−0.39	+1.98	2.75	−0.004
148.149.154	166.29	+1.08	−0.83	+0.25	1.90	0
149.151.154	164.12	+0.87	−0.20	+0.66	1.07	+0.002
151.154.155	154.97	+0.89	−1.87	−0.98	2.77	+0.004
151.155.157	165.05	+1.62	−3.19	−1.57	4.81	−0.003
151.157.160	171.26	+1.43	−1.82	−0.39	3.25	+0.001
157.159.160	174.96	+0.73	−1.86	−1.13	2.59	+0.001
159.160.161	140.52	+1.33	−0.44	+0.89	1.77	−0.004
160.161.162	123.07	+1.62	+0.23	+1.85	1.39	−0.005
161.162.163	135.97	+1.38	+0.19	+1.57	1.19	−0.003
162.163.164	111.25	+1.24	+0.85	+2.09	0.39	−0.005

$\dot{\varepsilon}_1, \dot{\varepsilon}_2$: Principal strain rate per year, obtained from $\varepsilon_1 = F - 1$ and $\varepsilon_2 = G - 1$. A positive sign indicates a tension and a negative sign a compression in this paper. The strains ε_1 and ε_2 signify respectively the algebraically maximum and minimum values among the strains in the whole directions.

$\dot{\Delta}$: Rate of change in area of a triangle per year, i. e., surface dilatation, obtained from $\Delta = FG - 1$.

$\dot{\gamma}_{max}$: Maximum shear strain rate per year, obtained from $\gamma_{max} = (F^2 - G^2)/2FG$. The directions of it are $\alpha \pm 45°$.

$\dot{\omega}$: Rate of clockwise rotation of the principal axes per year, obtained from $\omega = \alpha' - \alpha$, where α' is the direction of the major axis of the strain ellipse.

An observed error in each length of a side was estimated to be smaller than 0.04 m, which gave the mean square error of strain rate smaller than 10^{-5} per year.

Detailed values concerning the strain parameters are presented in Table 2, as reproduced from another article by NARUSE (1978).

Ⅳ. Distribution of horizontal flow velocity and surface strain

Ⅳ. 1. *Distribution of flow vector and principal strain*

A general view of the ice flow across the triangulation chain is shown in Fig. 12. Each arrow represents the horizontal vector of the ice flow averaged over several stations. It is clear that the flow is converging into the Shirase Glacier.

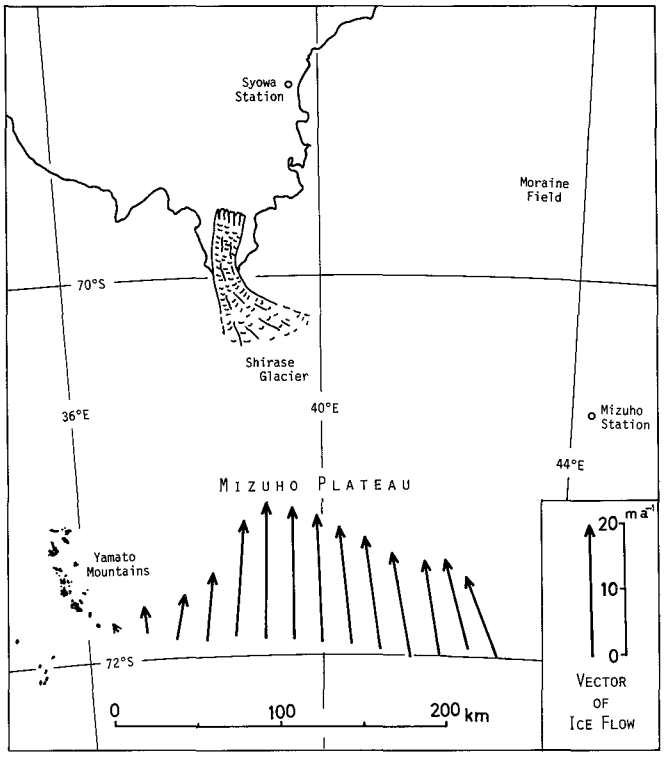

Fig. 12 Distribution of horizontal vectors of ice flow (m a^{-1}) along the triangulation chain. Each arrow represents the average value among several stations around it.

Horizontal flow vectors (m a^{-1}) and principal strain rates (a^{-1}) of the snow or ice surface along the triangulation chain were distributed, as shown by arrows in Figs. 13, 14, 15 and 16, with the topographic contours of the surface relief. The 10-m interval contour lines are based on the results of triangulation survey and observation of surface slopes of the ice sheet, as mentioned in Section V.

Remarkable features of the distribution of flow and strain are summarized as follows :

(1) The flow velocity had such small values as were less than 2 m a^{-1} and the flow direction was northwestward in the vicinity of the Yamato Mountains, namely the region from A003 to A020 (see Fig. 13). The small value is considered to be caused by the effect of many nunataks lying downstream. As a consequence, the mode of ice deformation was longitudinally compressive, as seen in the pattern of the principal strains in the west part in Fig. 13.

(2) Large tensile strains along the direction from SSW to NNE were noted near A020 (see Fig. 13). The fact is compatible with the existence of large-scale crevasses which run along the direction from WNW to ESE.

(3) The direction of the ice flow was different from one another on either side of A032 at 37°E in longitude (see Fig. 13). To the west of A032, the flow had a westward component, while to the east of it up to A075, the flow had an eastward component. The macro-scale surface contours of the ice sheet showed a ridge around the boundary (SHIMIZU *et al.* 1978a). It must follow, therefore, that an ice divide exists near 37°E between the drainage of the Shirase Glacier and the drainage at its west side.

(4) The flow velocity increased gradually with an increase in distance from the datum point up to A069, that is from west to east (see Figs. 13 and 14). It was more than 10 m a^{-1} at

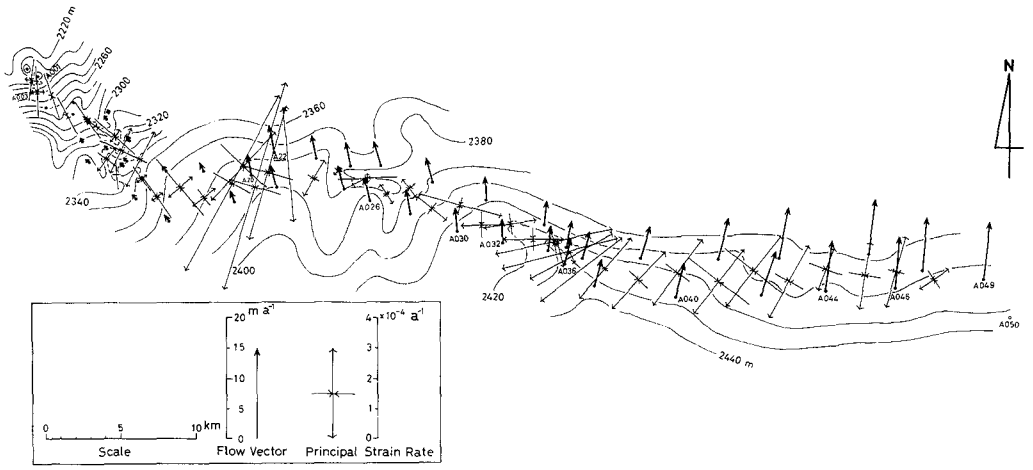

Fig. 13 Distribution of horizontal vectors of ice flow (m a^{-1}) and principal strain rates $\dot{\varepsilon}_1$ and $\dot{\varepsilon}_2$ (a^{-1}) in the region from A001 to A049. Surface contour lines are marked every 10 m.

A051 and more than 20 m a^{-1} in the region between A065 and A081 (see Fig. 14). The maximum value was observed to be 21.3 m a^{-1} at A069 (39°10'E).

(5) The value of velocity decreased slightly starting at A070 (see Fig. 14) and reached 13.6 m a^{-1} at A164 which was located at the east end of the triangulation chain (see Fig. 16).

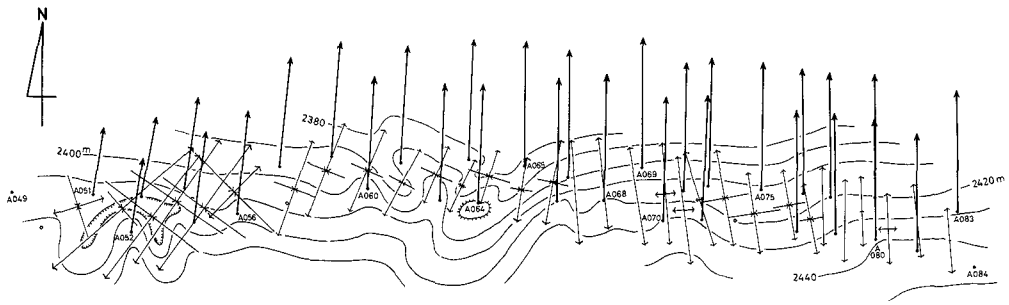

Fig. 14 Distribution of horizontal vectors of ice flow (m a^{-1}) and principal strain rates $\dot{\varepsilon}_1$ and $\dot{\varepsilon}_2$ (a^{-1}) in the region from A050 to A083. Surface contour lines are marked every 10 m. Scales are shown in Fig. 13.

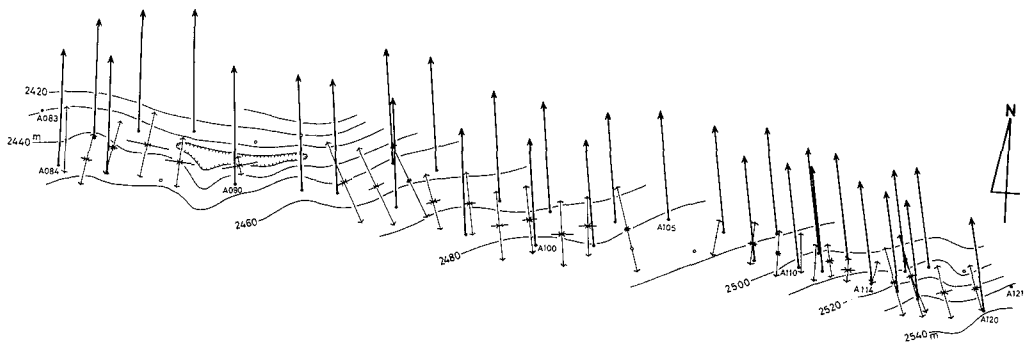

Fig. 15 Distribution of horizontal vectors of ice flow (m a^{-1}) and principal strain rates $\dot{\varepsilon}_1$ and $\dot{\varepsilon}_2$ (a^{-1}) in the region from A084 to A120. Surface contour lines are marked every 10 m. Scales are shown in Fig. 13.

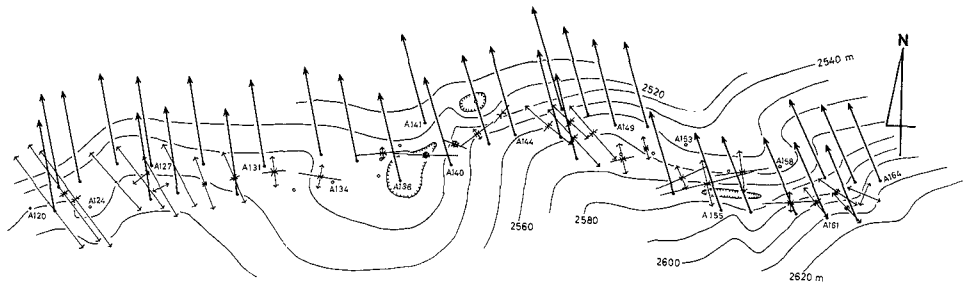

Fig. 16 Distribution of horizontal vectors of ice flow (m a^{-1}) and principal strain rates $\dot{\varepsilon}_1$ and $\dot{\varepsilon}_2$ (a^{-1}) in the region from A121 to A164. Surface contour lines are marked every 10 m. Scales are shown in Fig. 13.

(6) The direction of the ice flow pointed slightly eastward from north in the region from A033 to A075 (see Figs. 13 and 14) and slightly westward in the region from A076 eastward (see Figs. 14 and 15). The direction shifted gradually westward in the eastern part of the chain, and finally it was NNW at A164 (see Fig. 16).

(7) The direction and magnitude of the principal strains varied somewhat by the effect of the distinct surface undulation, as seen around the surface ridge at A036 (see Fig. 13) and the surface depression at A138 (see Fig. 16). However, the direction of the maximum extension was rather close to that of the surface flow. It represents that the mode of the ice flow was generally "extending flow" in this zone.

IV. 2. *Variations in flow velocity, dilatation, maximum shear strain, and rotation*

Figure 17 shows the variations in the horizontal component of flow velocity (m a^{-1}), the

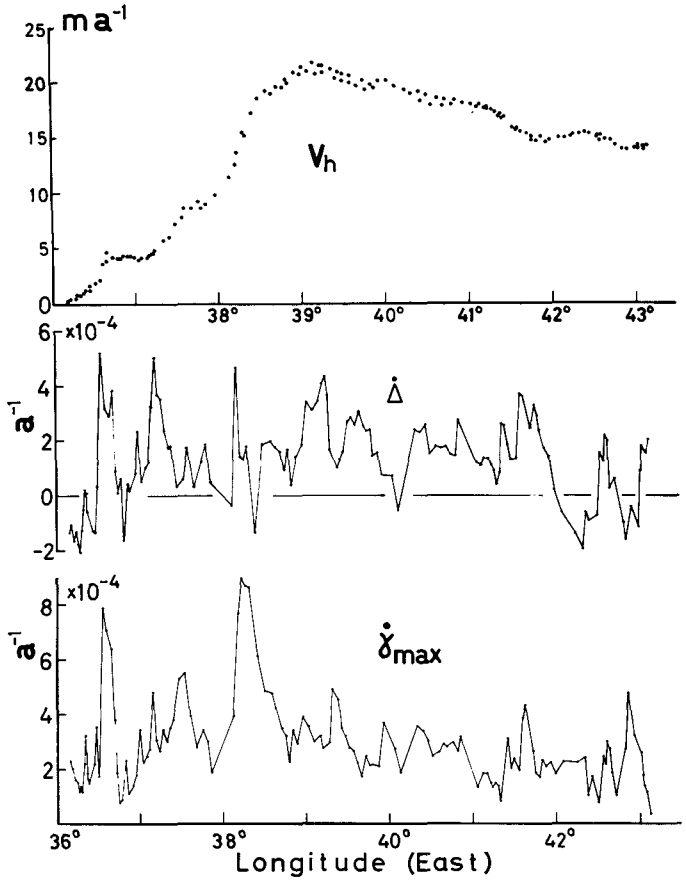

Fig. 17 Variations along the triangulation chain in the horizontal component of flow velocity V_h (m a^{-1}), the rate of surface dilatation $\dot{\Delta}$ (a^{-1}) and the rate of maximum shear strain $\dot{\gamma}_{max}$ (a^{-1}).

rate of surface dilatation (a^{-1}) and the rate of maximum shear strain (a^{-1}) plotted against the longitude from 36°10′E, the southeast end of the Yamato Muntains, to 43°10′E.

The spatial pattern of variation in the absolute value of velocity, which was mentioned in (1), (4) and (5) of the foregoing sub-section is more cleary shown in Fig. 17. A strong eastward increase in velocity exists in the region between 37°20′E and 38°30′E, but the region eastward from 39°10′E is marked by a gradual decrease. A slight scattering of values found around 39°E-41°E signifies the difference of velocities between the north-side and the south-side line of the triangulation chain ; namely, the velocity in the north side was higher than in the south side up to the value of several tens of centimeters per year. It follows that the ice flow was tensile along the direction of the flow, as observed in the distribution of the principal strains whose maximum extensions, namely ε_1, are oriented in such a direction as is approximately close to that of the ice flow.

The dilatation Δ shown in Fig. 17 is a two dimensional one, that is the ratio of change in area to the original area. If the absolute values of ε_1 and ε_2 are both small, neglecting the small quantity of the products $\varepsilon_1\varepsilon_2$, the dilatation is given as follows :

$$\Delta = \varepsilon_1 + \varepsilon_2. \tag{9}$$

The dilatation scattered considerably from place to place, but was generally positive except in the regions with surface depressions, as shown in Fig. 16.

The shear strain of the ice sheet surface at a station shows the maximum value in the direction $\alpha \pm 45°$. If the absolute values of ε_1 and ε_2 are both small, the maximum shear strain γ_{max} at a station is approximately equal to $\varepsilon_1 - \varepsilon_2$. It follows that γ_{max} shows a large value at

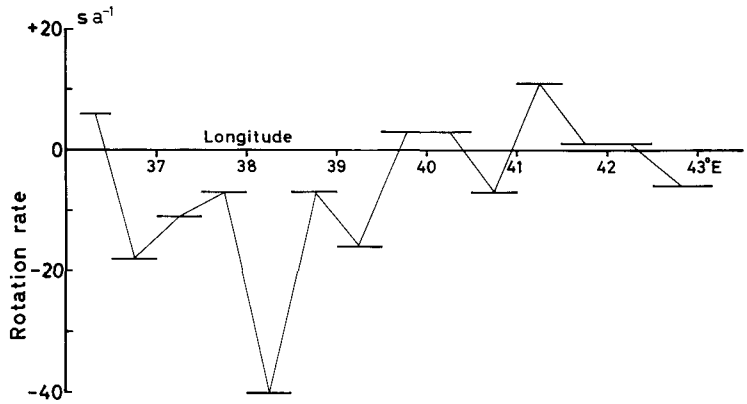

Fig. 18 Variation in the rate of rotation $\dot{\omega}$ (s a^{-1}) along the triangulation chain. The positive value shows clockwise rotation, the negative counterclockwise. Each segment represents the average value over every 30 minutes in longitude.

the place where the extension and contraction are both large. Such regions would correspond to those regions where the flow line converges or diverges considerably. The value of γ_{max} in Fig. 17 shows its peak at places where the horizontal velocity of the ice flow varies remarkably, i.e., at the regions around 36°30′E and 38°20′E. From the distribution of γ_{max}, a boundary between different modes of ice movement was deduced to exist around 38°20′E, while the surface divide of the drainages was determined at about 37°E, as mentioned before (see IV. 1. (3)).

Rates of rotation $\dot{\omega}$ gave rather large values such as 0.02 and 0.015 °a^{-1} respectively in the regions near 36°35′E and 38°20′E (see Table 2). These regions coincided well with those regions where the rates of shear strain were very large. In the other regions, rates of rotation were smaller than 0.01 °a^{-1}. The mean square error of the rate of rotation was estimated as ± 0.003 °a^{-1} at maximum. Only average values at every 30 minutes in longitude are shown in Fig. 18.

V. Relation between horizontal flow and topography

V. 1. *Classification of surface features*

With a view to examining a relation between the horizontal flow of surface ice and the topography of the ice sheet in this section, medium- or small-scale surface reliefs along the triangulation chain were classified into several categories.

Measurements of surface slopes of the ice sheet were carried out at every station of the triangulation chain : the vertical angle of the skyline was measured from a station by a theodolite in eight directions with 45-degree intervals and also in two additional directions of the maximum surface slopes, i. e., the downhill slope and the uphill slope. Suppose the measurement of the skyline is made on the sea surface and a theodolite is placed at 1.5 m in height, then the distance from the observation point to the horizon is 4.4 km in every direction. Meanwhile, on an undulating surface of the ice sheet, the distance to the horizon varies considerably with the direction due to the medium- or small-scale surface reliefs. The distance was approximately in a range from 1 km to 10 km in this surveyed region. Consequently, although the vertical angle of the skyline from a station does not provide specific information of the surface slope around it, the pattern of radial distribution of angles can be considered to show the surface feature of the ice sheet surrounding it.

Several typical examples of radial distribution of surface slopes are shown in Figs. 19 and 20. Dashed and solid lines indicate downhill and uphill slopes, respectively, while the length of the radius represents the surface slope in minutes. The figures typify the surface features : Fig. 19 shows a sheet with a smooth slope (A069 and A105), a complex undulation like a saddle point (A007), and a surface with a crooking maximum slope (A022) ; Fig. 20 shows a mound

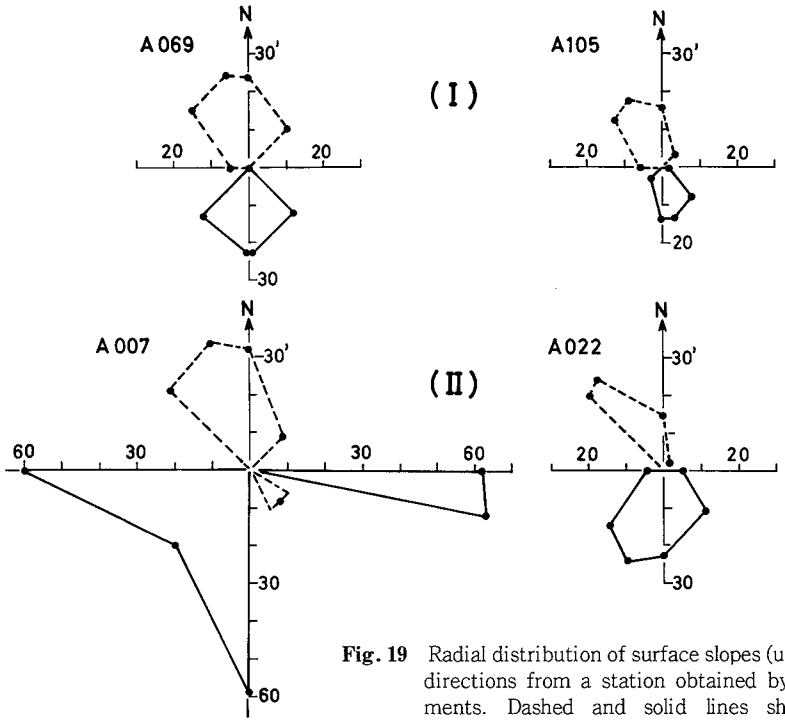

Fig. 19 Radial distribution of surface slopes (unit : minute) in ten directions from a station obtained by skyline measurements. Dashed and solid lines show the negative (downhill) and the positive (uphill) slope, respectively. (I) Sheet with smooth slope ; (II) Irregular undulation.

(A036), a ridge (A052), and a trough or depression (A138 and A158). Surface reliefs around stations could be classified into the four characteristic types, considering (a) the difference in directions between the uphill and the downhill slope ; e. g., the smaller difference than 20 degrees refers to an even surface, (b) the difference in magnitude of slope between the uphill and the downhill slope ; e. g., the smaller difference than 30 minutes refers to an even surface, (c) the number of directions of uphill slopes among the eight directions ; e. g., the large numbers of 6, 7 and 8 refer to the concave surface and the small numbers of 0, 1 and 2 refer to the convex surface, and (d) the pattern of surface contour lines shown in Figs. 13, 14, 15 and 16. Four types of surface features are then designated and grouped as follows :

(1) Sheet with smooth slope (even surface) :

A023, A031, A035, A039, A043, A045, A047, A049, A051, A057, A059, A066, A067, A069, A070, A071, A073, A077, A080, A082, A084, A087, A089, A092, A097, A100, A101, A102, A105, A107, A108, A109, A110, A112, A120, A125, A126, A130, A144, A148.

(40 stations).

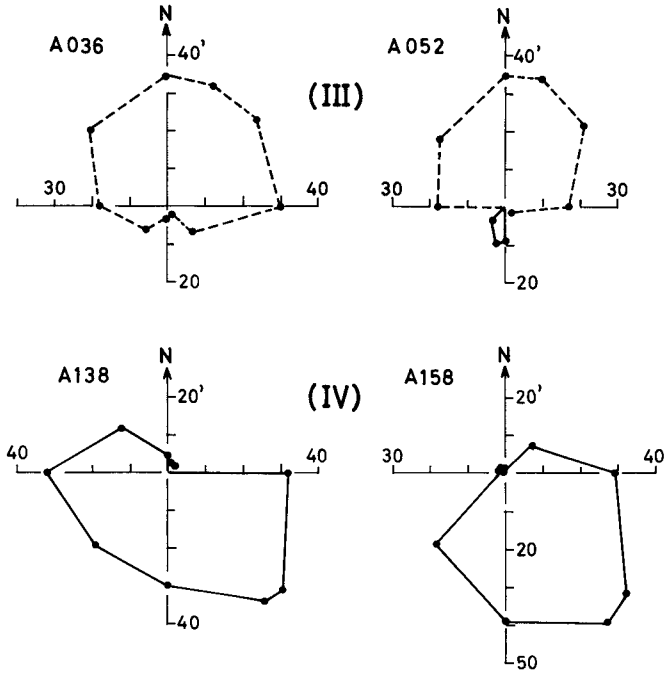

Fig. 20 Radial distribution of surface slopes (unit : minute) in ten directions from a station obtained by skyline measurements. Dashed and solid lines show the negative (downhill) and the positive (uphill) slope, respectively.
(III) Ridge or mound ; **(IV)** Trough or depression.

(2) Irregular undulation (saddle point or complex surface) :
A003, A004, A005, A007, A009, A011, A012, A013, A014, A015, A019, A021, A022, A027, A030, A061, A090, A094, A162.
(19 stations).

(3) Ridge or mound (convex surface) :
A010, A016, A020, A032, A036, A040, A044, A052, A056, A060, A064, A068, A072, A079, A083, A095, A111, A118, A127, A131, A147, A155, A159, A163.
(24 stations).

(4) Trough or depression (concave surface) :
A065, A074, A076, A088, A093, A119, A124, A132, A133, A134, A136, A137, A138, A139, A141, A143, A152, A153, A156, A157, A158, A160.
(22 stations).

As for other stations than those mentioned above, their surface reliefs indicated types intermediate between the four features.

The region to the west of A030 (37°E in longitude), that is near the Yamato Mountains, abounded in irregularly undulating surfaces, whereas the region to the east of A118 (41°30'E) abounded in ridges, mounds, troughs or depressions. It can be predicted that the bedrock topography has large and complex undulations in these two regions. Meanwhile, the surface features were relatively even in the region from A066 (39°E) to A112 (41°E), as is also clear from surface contour lines in Figs. 14 and 15. The bedrock surface is considered to be relatively smooth in this middle part of the triangulation chain.

The surface dilatation was generally positive on the ridge or mound, and negative on the trough or depression of the surface, while the maximum shear strain showed a large value on the surface with an irregular undulation. The amount of accumulation of snow was strongly controlled by the surface undulation, which will be described in Section VI.

V. 2. *Relation between directions of surface slope and flow*

A relation between the direction of the maximum surface slope β_s and that of the surface flow β_f was examined as for the 31 points on the ice sheet with smooth slopes classified above and also with the slope of more than 1/200, as shown in Fig. 21. The direction of a surface slope was obtained by averaging the direction of the maximum uphill slope and that of the maximum downhill slope from the data of skyline measurements (NARUSE 1975a). Differences in angles between the maximum slope direction β_s and the flow direction β_f are plotted along the triangulation chain in Fig. 22. The standard deviation of the value of $\beta_s-\beta_f$ was only 9 degrees. From this analysis, it is concluded that the direction of the ice flow coincides approximately with that of the maximum surface slope on the sheet with a smooth slope. Ice should, therefore, flow in the direction of the maximum surface slope even though the bedrock inclines in the opposite direction. This is a useful result for predicting a flow line from the measurement of surface topography, as was used conventionally (e. g., GIOVINETTO 1964).

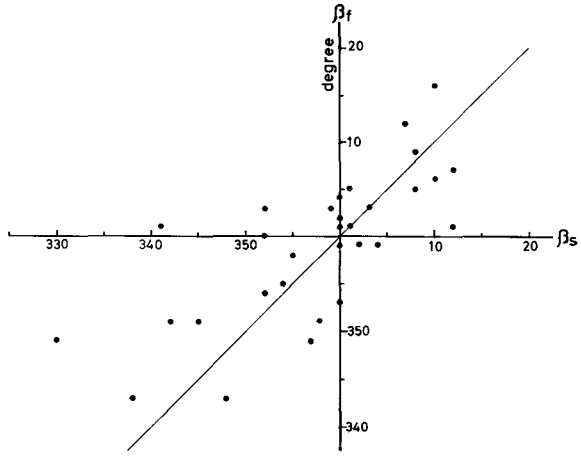

Fig. 21 Relation between direction of maximum surface slope β_s (degree) and that of surface flow β_f (degree). Both directions are represented clockwise from north. The values were obtained at the 31 triangulation stations on smooth slopes with the maximum slope of more than 1/200 ($\simeq$ 17 minutes).

Large discrepancies between the two directions were, however, observed at points on mounds, depressions and irregularly undulating terrains. These results showed that ice may

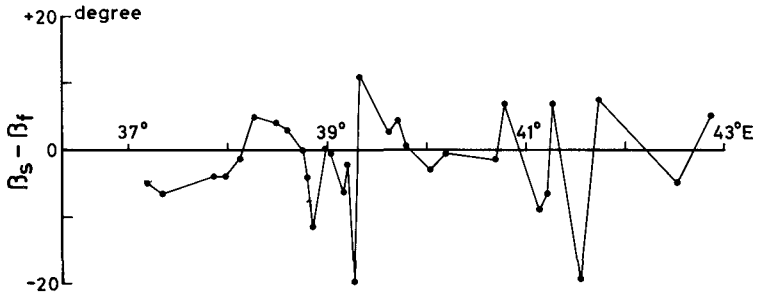

Fig. 22 Variation along the chain in difference (degree) between directions of maximum surface slope β_s and ice flow β_f. The values were obtained at 31 triangulation stations on smooth slopes with the maximum slope of more than 1/200.

flow along the general maximum surface slope around the point, not along the slope of a small-scale surface relief such as the undulation of a few kilometers in a horizontal dimension.

V. 3. *Profile of bedrock relief*

Measurements were made of ice thickness by radio echo soundings intermittently at triangulation stations in 1969 and 1973-1974. The results were published by SHIMIZU *et al.* (1972) and by NARUSE and YOKOYAMA (1975). The electromagnetic wave velocity of 171 m$(\mu s)^{-1}$ (CLOUGH and BENTLEY 1970) was used to calculate the ice thickness. SHIMIZU *et al.* (1978a) showed a bedrock profile along the triangulation chain, assuming simply that an echo with the longest echo time was the reflected one from the bedrock surface. It remains a possibility, however, that the one with the longest echo time among multiple echoes is not necessarily the one from the bedrock just beneath a transmitting station. ROBIN (1975) pointed out some problems in interpreting of radio echo signals, and GUDMANDSEN (1975) showed a multitude of extensive layers within the Greenland ice sheet. Moreover, the phenomenon of the spatial fading of an echo due to the irregularity of the bedrock surface has been much discussed by many investigators (e.g., OSWALD 1975). MAE (1978) reexamined the multiple echoes obtained along the traverse routes in Mizuho Plateau, whereby he put forth bedrock profiles which he considered as more reasonable ones. Nevertheless, it is still necessary to check the ice thickness data.

Therefore, raw data of ice thickness at triangulation stations were examined using the values of free-air anomaly obtained by YOSHIDA and YOSHIMURA (1972) and by ABE (1975). Such a value of thickness that was discrepant with the free-air anomaly in the trend of their variations from station to station was regarded to be possibly erroneous due to misinterpreting of the true echo from the bedrock. Hence, upon elimination of these ice thickness data, only probable thicknesses are tabulated in Table 1 (Section III). The obtained profile of the bedrock surface along the triangulation chain is shown in Fig. 23. The profile is discontinued at places

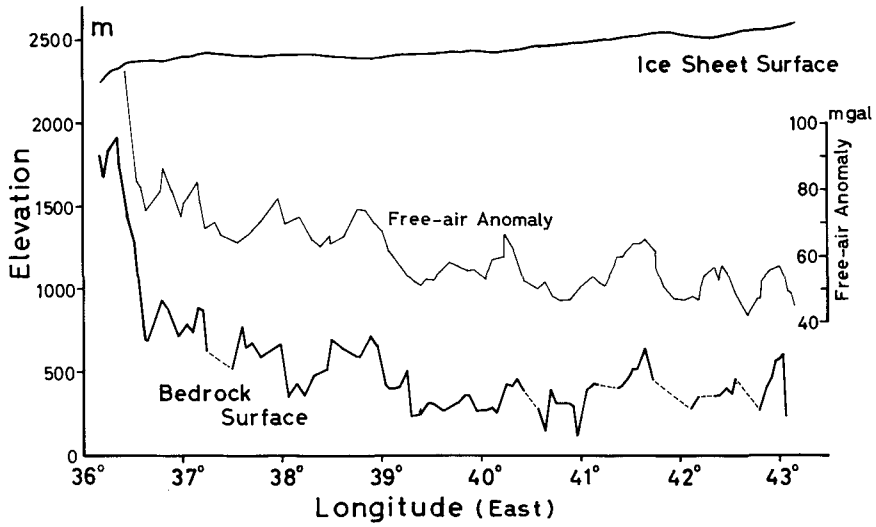

Fig. 23 Profiles of the ice sheet surface, bedrock surface and free-air anomaly of gravity along the triangulation chain in the parallel of 72°S. Bedrock elevations were obtained by radio echo soundings.

where the thickness data were eliminated. Ice thicknesses with solid lines are only used in calculations in the following sections. Also shown in Fig. 23 are profiles of the ice sheet surface and of free-air anomaly.

The mean thickness of the ice sheet was about 1600 m near the Yamato Mountains, that is the west side from 38°E in longitude, while it was about 2100 m in the region between 38°E and 41°E. As described in Sub-section V. 1., the bedrock surface may be heavily undulating in the eastern region from 41°30'E. Most of thickness data were eliminated in this region. It is difficult to measure the accurate thickness from intermittent echo soundings at such an area over the ice sheet that has a complex bedrock relief. Since the profile of gravity is not reflected by minor irregularities of the bedrock (DREWRY 1975), it remains possible that sub-glacial mountains exist in the region from 41°E to 43°E. If so, a sub-glacial trough, which must be one of the main tributary flows of the Shirase Glacier, is inferred to run across the region from 39°E to 41°E. The surface velocity of the ice flow was largest in this region, its value being 17–21 m a^{-1}.

The same method as described above was also used to examine ice thickness data along Route C in 71°S (see Fig. 1) which is located about 100 km downstream from the triangulation chain in 72°S. The bedrock surface obtained from radio echo soundings in 1970 (SHIMIZU *et al.* 1972) is shown by a dashed line in Fig. 24. No echo pulses were observed in 1970 in the regions around the distances of 110 km, 170 km and 240 km from the Yamato Mountains. A number of multiple echoes were obtained from shallow levels in the measurements in 1973 in these

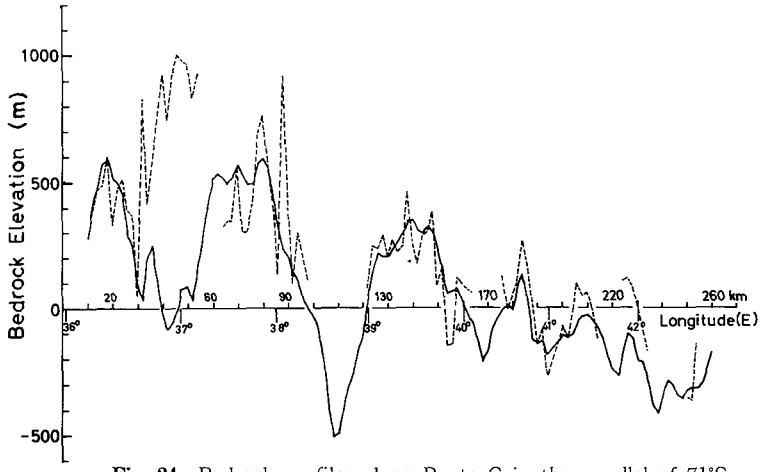

Fig. 24 Bedrock profiles along Route C in the parallel of 71°S. Distance in kilometers is taken from the northeast end of the Yamato Mountains. A profile in a dashed line was obtained by radio echo soundings carried out in 1970 ; a profile in a solid line was calculated from gravity values.

regions (NARUSE and YOKOYAMA 1975). Such echoes were regarded as those originating in others than the bedrock surface, as the result of examining of the distribution of free-air anomaly. ABE *et al.* (1978) obtained a distributional map of the Bouguer anomaly Δg_0" in Mizuho Plateau from the following equation :

$$\Delta g_0" = g + 0.1967H + 0.0742I - \gamma_0, \tag{10}$$

where g is the observed gravity value (mgal), H the elevation (m), I the ice thickness (m), and γ_0 the standard gravity value (mgal) determined only by the latitude of the station. Densities of ice and bedrock were assumed as 900 kg m^{-3} and 2670 kg m^{-3} respectively. ABE *et al.* showed that Δg_0" was approximately constant as -70 mgal in the entire region along Route C. The thicknesses I at the gravity stations along Route C were then calculated from eq. (10), assuming that $\Delta g_0" = -70$ mgal there. The obtained profile of the bedrock surface along Route C was represented by a solid line in Fig. 24. A large discrepancy between the two profiles in Fig. 24 appeared in the region at the distance from 30 km to 60 km (around 37°E). This region is marked by a trough on the basis of gravity values, whereas it has a sub-glacial rise according to radio echo soundings. In other regions than the above, the two profiles almost coincide with one another.

Clearly noticed from the calculated bedrock profile is that deep sub-glacial troughs lower than the sea level exist around the distances of 110 km, 170 km and 240 km, where radio echoes were not recieved in 1970. Deep troughs were found around 38°40′E and 40°30′E $-$41°E in 71°S by seismic measurements made in 1960 (ISHIDA 1962). The former trough should correspond to the deep trough 500 m below sea level at the distance of 110 km (38°40′E) in Fig. 24. Consid-

ering also the flow line of ice described in Section VII, a small-scale trough crossing the parallel of 72°S at 38°10′E, as seen in Fig. 23, can be inferred to link with the deep trough at the distance of 110 km in Route C, namely 38°40′E in 71°S. The mean slope of the bedrock surface is estimated as 1/100～1/200 in the area from 72°S to 71°S, while the mean slope of the ice sheet surface is about 1/150.

V. 4. *Empirical relation of surface velocity*

Based on a simplified model of a glacier, the surface velocity resulting from the deformation of an ice mass in simple shear is derived by NYE (1952) from the flow law of ice (GLEN 1955), namely $\dot{\gamma}=A\tau^n$, where $\dot{\gamma}$ is the shear strain rate, τ the shear stress, and A and n the parameters. The shear stress on a layer at a depth z is represented approximately as $\tau = \rho g z \sin\theta_s$, where g is the gravitational acceleration, ρ the density of ice, and θ_s the surface slope. The shear strain rate $\dot{\gamma}$ is here $\frac{1}{2}\mathrm{d}v/\mathrm{d}z$, where v is the horizontal velocity. It then follows, by integration, that the surface velocity V_h is given by

$$V_h = V_b + \frac{2A}{n+1}(\rho g \sin\theta_s)^n \cdot I^{n+1}, \tag{11}$$

where V_b is the velocity at the bedrock surface and I the ice thickness. Equation (11) is sometimes called the laminar flow formula, because the flow lines are parallel to the surface of the ice sheet.

We now obtain an empirical simple relation of the surface velocity based on eq. (11), which will be fit for the ice sheet of Mizuho Plateau. NISHIO and MAE (1979) calculated the steady state temperature distribution within the ice sheet along the triangulation chain, then the temperature at the base was given as −3°C or −8°C under the following condition ; namely, the surface temperature : −35°C ; surface velocity : 20 m a^{-1}; ice thickness : 2000 m ; annual net accumulation : 0.05 m a^{-1} or 0.10 m a^{-1} in water equivalent ; geothermal heat flux : 4.2×10^{-2} J m^{-2} s^{-1}. From this, it can be considered that the basal ice is below the pressure melting point and does not slide on its bed in most part of the triangulation chain. The velocity V_b is, therefore, taken as 0 in eq. (11).

Twenty-three stations were selected from the triangulation stations, which satisfied the following three conditions :

(1) The surface feature shows the sheet with a smooth slope as defined in Sub-section V. 1.

(2) The difference in directions is small between the maximum surface slope and the ice flow, as described in Sub-section V. 2.

(3) The value of ice thickness obtained by radio echo soundings is reliable, judging from the gravity value, as shown in Sub-section V. 3.

Substituting the values of n from 1.0 to 4.0 into eq. (11), the relation was examined between the measured values of V_h and the values of $(\sin\theta_s)^n \cdot I^{n+1}$ at the above 23 stations along the triangulation chain. The value of θ_s taken is the surface slope along the direction of

the ice flow (see Table 1). A correlation between V_h and $(\sin\theta_s)^n \cdot I^{n+1}$ was slightly better in the case in which n was equal to about 2. Figure 25 shows the relation between V_h and $(\sin\theta_s)^2 \cdot I^3$. The correlation coefficient between these values was 0.83, while the relative standard deviation, i. e., the standard deviation of the calculated value $(\sin\theta_s)^2 \cdot I^3$ from a regression line divided by the mean value of $(\sin\theta_s)^2 \cdot I^3$, was 0.20.

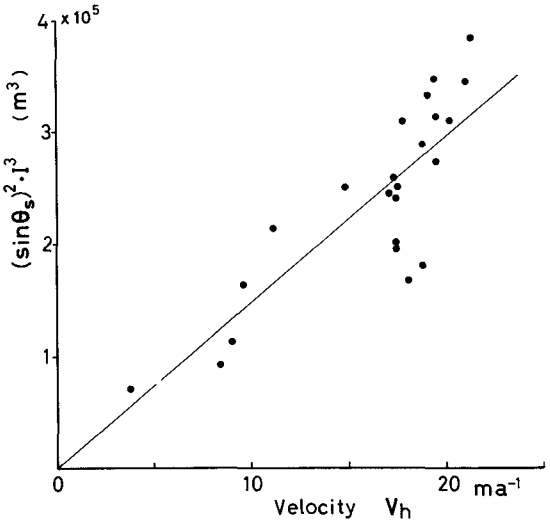

Fig. 25 Relation between measured values of horizontal velocity V_h (m a^{-1}) and calculated values of $(\sin\theta_s)^2 \cdot I^3$ (m^3) at 23 triangulation stations on smooth slopes.
θ_s : Mean value of the uphill and the downhill slope of the ice sheet surface (degree) obtained by skyline measurements.
I : Ice thickness (m) obtained by radio echo soundings.

The value of A in the flow law depends on ice temperature. Measured and computed temperature profiles in the Greenland and the Antarctic ice sheet showed that the ice temperature is approximately constant in the upper half of the ice sheet and increases steeply near the base (ROBIN 1976, UEDA and GARFIELD 1968). Therefore, eq. (11) with the constant value of A cannot be applied over the entire depth of the ice sheet in a strict sense. However, the error due to this rough approximation of the constant A should be included within the scattering of values in Fig. 25. Allowing the error (standard deviation) of 20 %, the obtained empirical relation can be used to predict the surface velocity from the data of the surface slope and ice thickness, as is shown in Sub-section VII. 3.

The parameter n does not depend on ice temperature, but on the mode of its deformation. PATERSON (1969) concluded from the experimental results obtained by many investigators that values of n for polycrystalline ice varied between 1.9 and 4.5 with the mean of about 3. In glacier studies, n is commonly assumed to be 3. But, there are some indications that n is reduced to about 2 or even 1 for low stresses (BUTKOVICH and LANDAUER 1960). The basal shear stress τ_b calculated from $\tau_b = \rho g I \sin\theta_s$ showed low values from 0.6 bar to 1.2 bars in the region along the triangulation chain. The mean value of τ_b was about 1 bar, which was nearly the same as the value commonly obtained in the Antarctic ice sheet (e. g., ROBINSON 1965). HUGHES (1973) suggested that for polycrystalline ice n is 1.5 as the minimum value for single maximum fabrics and n is 3.0 as the average value for random fabrics (mixed basal and prismatic glide). It is possible that the fabrics of ice have a preferred orientation and cause a basal glide in the lower part of the ice sheet. The above two effects,

namely the low stress and the preferred orientation, may be considered to account for the adoption of a value of about 2 as n.

VI. Vertical flow and local mass budget deduced from it

VI. 1. *Distribution of annual net accumulation*

The surface mass balance measured by stakes in thickness of snow is called simply "net accumulation" and is denoted by A_n in this paper. Annual net accumulations averaged over four years were obtained at 133 triangulation stations from the stake measurements carried out in 1969 and 1973-1974. The results are shown in Table 1 (Section III). At places where the stakes could not be found in the resurvey, net accumulations over four years were regarded as larger than the original height of the stakes, since the stakes were considered to have been buried under the accumulated snow. Annual net accumulations at these stations were estimated as follows : more than 0.35 m a^{-1} at A050, A058, A074, A088, A104, A106, A124, A134, A136 and A152 ; more than 0.40 m a^{-1} at A132 and A150 ; more than 0.45 m a^{-1} at A091 and A093 ; more than 0.50 m a^{-1} at A119, A137, A143, A153, A156 and A158 ; more than 0.55 m a^{-1} at A139.

Distribution of annual net accumulation A_n (m a^{-1}) is shown along the chain in Fig. 26, in which the running mean over five stations was applied. As for places where stakes were missing, the foregoing possible minimum values plus 15% of them were also counted in the running mean. It is noted from Fig. 26 that the net accumulation was negative in the region to the west of 36°50'E, i.e., near the Yamato Mountains. Since the ice sheet surface was not

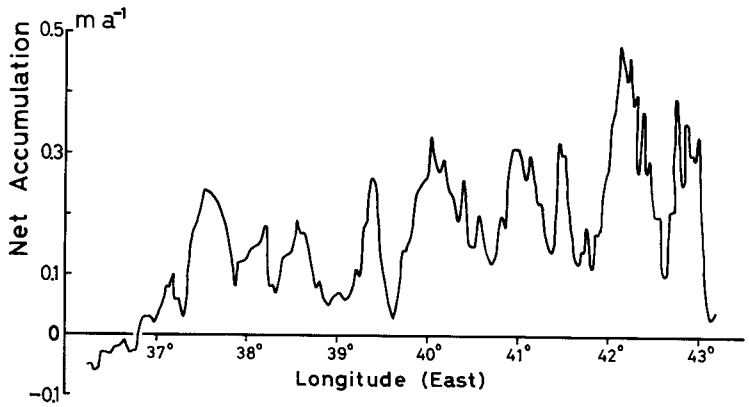

Fig. 26 Distribution of annual net accumulation (m a^{-1}) in thickness of snow along the triangulation chain measured by snow stakes. Running mean over five stations was applied.

covered by snow but was mostly composed of ice in this region, the amount of annual ablation was represented by the thickness of ice in Fig. 26. Ablation of ice is considered due mainly to sublimation of ice. The mean annual net accumulation in the region from 37°E to 43°E was 0.20 m a^{-1} in snow depth. Assuming the average density of surface snow as 450 kg m^{-3} (NARUSE 1975b, WATANABE 1975), the annual net accumulation was 90 kg $m^{-2}a^{-1}$ in water equivalent.

Also noticed from Fig.26 are remarkable variations of net accumulation from place to place. These areal variations were observed in every route of measurements in Mizuho Plateau (YAMADA *et al.* 1978). A strong correlation was seen between the amount of net accumulation and the topography of the ice sheet surface. Figure 27 shows histograms of the annual net accumulation among stations in smooth slopes, among those in mounds or ridges, and among those in troughs or depressions, which are defined in Subsection V. 1. It is evident that net accumulations were great in troughs or depressions, where almost all the values were more than 0.40 m a^{-1}. Difference in accumulations was little between on the mounds (or ridges) and on smooth slopes. The mean net accumulation was 0.47 m a^{-1} in thickness of snow at the depressed terrain, 0.12 m a^{-1} at the smoothly sloped terrain, and 0.09 m a^{-1} at the mound terrain. Snow particles transported by strong katabatic winds are considered to have deposited in a large amount at the depressed surface, where the wind speed was relatively small. Such an irregular distribution of accumulations makes the undulating surface smooth, in case the ice flow is parallel to the surface, namely there is no emergence or submergence flow of ice.

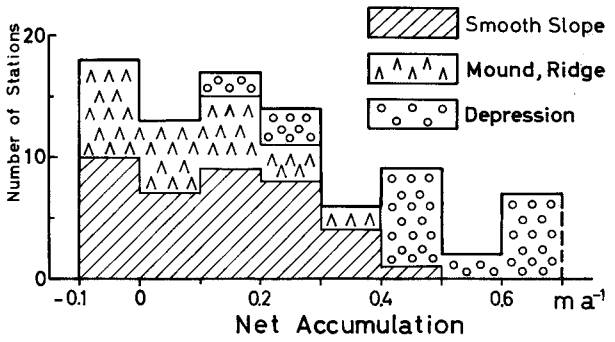

Fig. 27 Histogram of the amounts of annual net accumulation (m a^{-1}) in thickness of snow at different surface features ; namely, smooth slope, ridge or mound, and trough or depression.

VI. 2. *Variation in emergence or submergence velocity*

The emergence or submergence velocity V_z (m a^{-1}) at the surface which was obtained by eq. (8) is plotted in Fig.28 against the longitude along the chain from the southeast end of the Yamato Mountains to A164 (S240). The variation in V_z was slightly smoothed out by the application of the running mean over three stations. The following results are characteristic of V_z:

(1) Positive velocities which signify an emergence flow of ice were obtained in the re-

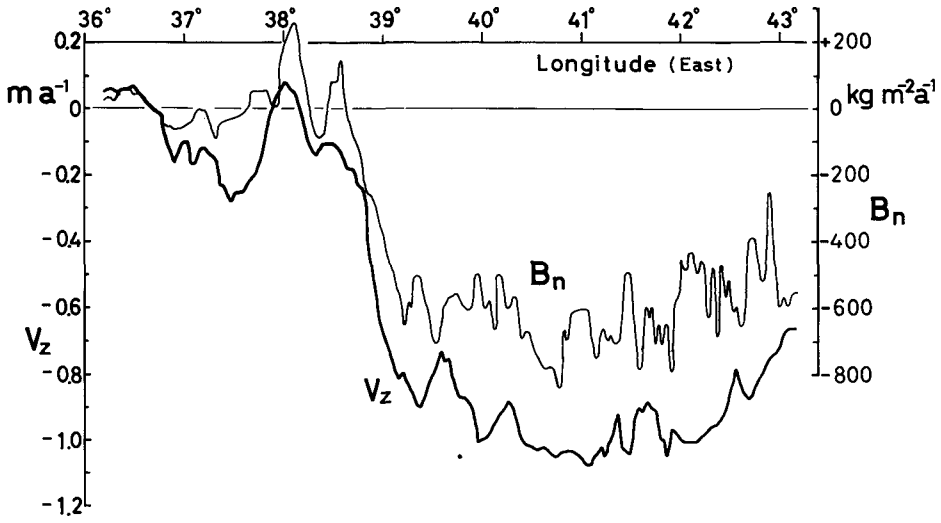

Fig. 28 Variations in emergence or submergence velocity V_z (m a^{-1}) and local net mass budget B_n (kg m^{-2} a^{-1}) along the triangulation chain. Running means over three stations were applied to V_z and B_n.

gions around 36°30′E and 38°E. An annual net accumulation was negative in the former region near the Yamato Mountains, which represents ablation due mainly to sublimation of the exposed surface ice. It is consistent with the emergence flow often observed in the ablation area of a glacier. A large number of meteorites were found (YOSHIDA *et al.* 1971, SHIRAISHI *et al.* 1976, YANAI 1978, MATSUMOTO 1978) in this region, which, therefore, was named the Meteorite Ice Field. It is considered that the meteorites were exposed at the ice surface as the results of the emergence flow and sublimation of ice (NAGATA 1978, NARUSE 1979).

(2) In most part except the above regions, negative velocities indicative of a submergence flow were observed and net accumulations were positive. The submergence velocity increased suddenly near 39°E where the horizontal velocity was close to the maximum value (see Fig.17), and then it decreased gradually from 42°E eastward. The value of V_z reached -1.0 m a^{-1} in the region between 40°E and 42°E, where the mean square errors of V_z were from ± 0.25 m a^{-1} to ± 0.30 m a^{-1}, as shown in Table 1.

VI. 3. *Local mass budget at each triangulation station*

It was shown in the preceding seb-section (Fig. 28) that the submergence velocity of the surface was nearly -1.0 m a^{-1} in the region from 40°E to 42°E. The average net accumulation there is estimated as 0.2 m a^{-1} in thickness of snow from stake measurements at 44 triangulation stations in the period from 1969 to 1973. Therefore, taking into account the maximum probable error in the velocity estimation (0.25 m a^{-1}), the supply of snow on the ice sheet

surface is not sufficient to maintain a stable profile of the ice sheet. It is probable that the ice sheet should have been thinning in the region during this observation period.

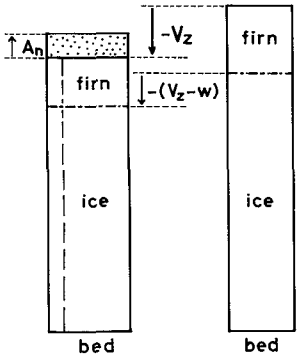

Fig. 29 A schematic figure showing the contraction of the ice sheet along the vertical direction, which resulted from the densification of firn layer and the outflow of ice.

We now introduce a new concept, "local mass budget" or "mass budget density", at each triangulation station. Suppose a vertical column with a unit cross area from the surface of the ice sheet to the bedrock, as illustrated in Fig. 29. The downward motion of the surface results from densification of the upper firn layer, which includes contraction of bubbles in ice, and also from the outflow of ice from the column to the surrounding area, while the upward motion of the surface results from the inflow of ice into the column. The local net mass budget per year at each station is defined by the difference between the annual income of an ice mass to the vertical column fixed to the bed and the annual outgo of an ice mass from the column. Densification does not cause any change in the mass of the column. Since the ice of density ρ_i is incompressible, an ice mass of $-(V_z-w)\rho_i \cdot a \cdot t$ should be drained from the column, where w is the rate of surface lowering per year due to densification of the upper layer of the ice sheet, a is a unit cross area of the column, and t is the number of years (one year in terms of annual drainage). Assuming that no melting of ice occurs at the bottom of the ice sheet, the local net mass budget B_n (kg $m^{-2}a^{-1}$) is given as follows :

$$B_n = A_n\rho_s + (V_z - w)\rho_i, \tag{12}$$

where A_n is the thickness of annual net accumulation and ρ_s is the density of deposited snow on the surface. One should take notice of signs of terms in eq. (12) : the positive B_n signifies the gain of a mass and the negative B_n the loss ; the positive V_z corresponds to the upward flow and the negative V_z the downward ; w is always negative.

The vertical distribution of density was obtained by NARITA and MAENO (1978) from the surface down to 124 m at Mizuho Station (70°42′S ; 44°20′E ; 2230 m a. s. l.). The density increased gradually from 400 kg m^{-3} at the surface to 820 kg m^{-3} at 50 m and 890 kg m^{-3} at 120 m below the surface. It is considered that most of densification occurs in the upper 100 m of the ice sheet in the inland area of Mizuho Plateau.

The value of w is unknown at the respective triangulation station. Hence, we assume that the accumulation rate at each station is constant with time and that the function $\rho = f(h)$, describing the density-depth relationship, is invariant with time (SORGE's law), where ρ is the density and h is the depth below the surface. Then, if a volume of snow at h sinks by dh in a time dt, the equation $A_n\rho_s dt = \rho(h)dh$ holds, since the density-depth curve is invariant with

time (BADER 1960, 1962). The downward velocity of a snow particle, $W(h)$, at any depth h relative to the snow surface is given by

$$W(h)=-\frac{dh}{dt}=-\frac{A_n\rho_s}{\rho(h)}. \tag{13}$$

It follows that $W(0)=-A_n$ at the snow surface and $W(h_i)=-A_n\rho_s/\rho_i$ at the depth h_i where the density becomes ρ_i. Hence, we obtain the rate of surface lowering w due solely to densification of the upper layer of the ice sheet as

$$-w=A_n-A_n\frac{\rho_s}{\rho_i}. \tag{14}$$

Substituting w into eq. (12), we get

$$B_n=(A_n+V_z)\,\rho_i. \tag{15}$$

Now, taking ρ_i as 900 kg m^{-3}, the local net mass budget B_n was calculated from eq. (15) at each triangulation station. The variation in B_n is shown in Fig. 28, together with V_z. In the region from 39°E westward, B_n was close to 0 kg m^{-2}a^{-1} ; while in the region from 39°E eastward to 42°E, it showed a large negative value, showing a substantial mass deficit, namely the value from -500 to -800 kg m^{-2}a^{-1}. It follows that the ice sheet is in a steady state in the western region of the triangulation chain near the Yamato Mountains. On the other hand, it is in an unsteady state and shrinking in the eastern region of the chain located in the middle part of the drainage of the Shirase Glacier. An index K, that is $(B_n/\rho_i I)$, which shows the ratio of the local net mass budget to the amount of stored ice, was obtained as -3.7×10^{-4} a^{-1} in the region from 39°E to 42°E.

The recent shrinking of the ice sheet observed does not necessarily mean to take place over the entire area of Mizuho Plateau. As for the entire ice in the drainage basin of the Shirase Glacier in Mizuho Plateau, SHIMIZU *et al.* (1978b) discussed the mass budget. The following estimations were made from the measurements in 1969-1975 : the drainage area : 20×10^{10} m^2 ; the stored ice : 32×10^{16} kg (SHIMIZU *et al.* 1978a) ; the total accumulation rate : $(13\pm8)\times10^{12}$ kg a^{-1} (YAMADA and WATANABE 1978) ; the annual discharge of ice through the Shirase Glacier : $(7.4\pm1.9)\times10^{12}$ kg a^{-1} (NAKAWO *et al.* 1978). We then obtained the mass budget of $(6\pm8)\times10^{12}$ kg a^{-1} by subtracting the discharge from the total accumulation, since the latter included the estimated amounts of melting at the coastal region and of drifting snow. Although the estimated error was not small, the mean value indicated a considerably large positive budget. The index K was about $+0.2\times10^{-4}$ a^{-1}. It is possible, therefore, that the observed intense thinning of the ice sheet in the region from 40°E to 42°E along 72°S should be a rather local occurrence.

FEDERER *et al.* (1970) also obtained the result of a mass deficit amounting to 0.10 m a^{-1} (corrected later as 0.077 m a^{-1} : FEDERER and SURY 1976) during ten years from 1959 to 1968 in the inclined shaft 40 m deep at Jarl-Joset Station in the inland Greenland ice sheet. Using the data, NYE (1975) showed the resultant lowering of the ice sheet surface. On the other hand,

PATERSON (1976) reported the recent thickening of an arctic ice cap of 0.1 m a^{-1} from the vertical strain rate measurements in bore holes near the crest of the Devon Island ice cap. As for the West Antarctica, some work has been done suggesting that the ice sheet is now disintegrating (HUGHES 1973, WEERTMAN 1976). THOMAS (1976) estimated that the West Antarctic ice sheet is currently thinning by about 0.4 m a^{-1} at Byrd Station, while WHILLANS (1973, 1976a, 1976b) stated, based on the analyses on continuity conditions and radio-echo layers, that the ice sheet is slightly thinning or close to a steady state. THOMAS (1976) showed that the Ross Ice Shelf is growing thicker by almost 1 m a^{-1} in the vicinity of its grounding line.

The results of the above studies in various regions suggest that the ice sheets and the ice shelves are not in a steady condition in response to recent climatic variations, mainly in precipitation. Moreover, the conditions as to stability of the ice sheet may considerably vary with the location.

Ⅶ. Conditions of ice flow over Mizuho Plateau

Ⅶ. 1. *Distribution of strains measured by square strain grids*

Quadrangle strain grids 1 km in each side were installed at nine stations over Mizuho Plateau in 1969-1970 (NARUSE *et al.* 1972). Seven of the grids were resurveyed during the period from 1970 to 1975 (NARUSE *et al.* 1972, SATOW 1977) at the following stations : S40, S100, S160, S200, C37, Y200, and Mizuho Station, their positions being shown in Fig. 32. Two grids at C80 and W55 were not found during the oversnow traverses in 1973-1975, probably because the stakes, originally about 2 m high above the snow surface, had been buried under the accumulated snow in a period of four years.

Methods of measurement and calculation of the surface strain of ice are the same as those made of the triangles in the chain. At each station strain parameters were calculated of each of the four triangles divided by two diagonals of the square. Obtained results are tabulated in another article (NARUSE and SHIMIZU 1978). Very close values of strain rates were obtained from the four triangles in all of the seven grids. Mean values at each station are shown in Table 3 as to the direction of the principal axis of the strain α, the principal strain rates $\dot{\varepsilon}_1$ and $\dot{\varepsilon}_2$, the surface dilatation rate $\dot{\Delta}$ and the maximum shear strain rate $\dot{\gamma}_{max}$.

Principal strain rates at the seven stations are shown on the configurations of the grids in Fig. 30. Strain rates at C37 and Y200 showed such small values as $2\sim5\times10^{-5}$ a^{-1}, comparable with the magnitude of observational errors, which are estimated as 2×10^{-5} a^{-1}. Such small strain rates were not observed of the triangles in the chain along 72°S, except in the region near the Yamato Mountains where the surface flow velocities were very small. The small strain rates at C37 and Y200 may be considered to have resulted from the very low horizontal velocities expected at the western and eastern fringes of the Shirase drainage basin. Tensile

strains were predominant, namely large positive dilatations, at S40, S100 and S200. Meanwhile, larger compressive strains than tensile strains in the absolute values were observed at S160 and Mizuho Station. It is noticeable that the maximum shear strain rate, i.e., approximately $\dot{\varepsilon}_1 - \dot{\varepsilon}_2$, was such a remarkably large one as 11×10^{-4} a^{-1} at S160, which suggested that flow lines there are converging considerably.

Table 3. Strain parameters of the ice sheet surface at the square strain grids. Explanations of the symbols are given in the text.
(after NARUSE and SHIMIZU 1978)

Station	Latitude (S)	Longitude (E)	Elevation (m)	α (degree)	$\dot{\varepsilon}_1$ (a^{-1})	$\dot{\varepsilon}_2$ (a^{-1})	$\dot{\Delta}$ (a^{-1})	$\dot{\gamma}_{max}$ (a^{-1})
S 40	69°04.7′	41°07′	1142	159.6	$+4.6\times10^{-4}$	$+0.4\times10^{-4}$	$+5.0\times10^{-4}$	4.2×10^{-4}
S 100	69°38.1′	42°50′	1680	108.8	+4.0	−0.9	+3.1	4.9
S 160	70°40.2′	43°06′	2058	105.9	+4.0	−7.2	−3.1	11.2
S 200	71°19.4′	43°00′	2309	158.5	+4.7	−2.1	+2.6	6.8
C 37	71°07′53″	37°27.5′	1853	74.1	+0.2	−0.5	−0.3	0.6
Y 200	71°46′13″	48°55′58″	2880	127.2	+0.4	−0.4	0.0	0.8
Mizuho Station	70°41′53″	44°19′54″	2230	117.1	+0.9	−4.0	−3.1	4.9

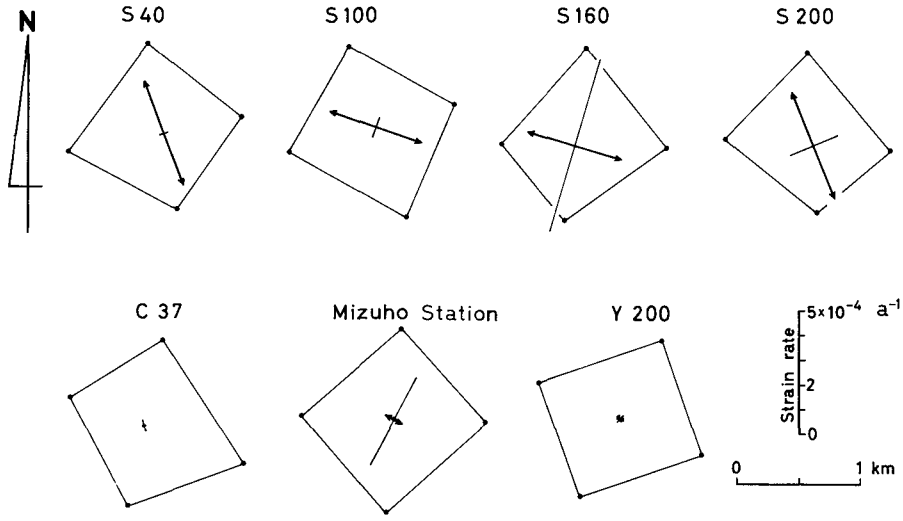

Fig. 30 Principal strain rates measured by means of square strain grids at seven stations over Mizuho Plateau. Arrows in thick lines indicate maximum extensions ; segments in fine lines indicate maximum compressions.

VII. 2. *Local mass budget deduced from strain measurement*

As is clear from Fig. 29, the submergence (emergence) velocity V_z at the surface indicates the thinning (thickening) rate of the vertical column through the ice sheet. The vertical strain rate of the ice sheet averaged over the thickness I, denoted by $\langle\dot{\varepsilon}_3\rangle$, is given by

$$\langle\dot{\varepsilon}_3\rangle=\frac{1}{I}\int_0^I\dot{\varepsilon}_3 dz=\frac{1}{I}\int_0^I\frac{\partial V_z(z)}{\partial z}dz, \tag{16}$$

where $V_z(z)$ is the velocity (at z) perpendicular to the surface. If it is assumed that V_z (0) at the bedrock surface is equal to 0, eq. (16) reduces to

$$\langle\dot{\varepsilon}_3\rangle=V_z/I. \tag{17}$$

The positive sign of $\langle\dot{\varepsilon}_3\rangle$ signifies thickening and the negative sign thinning.

The vertical strain rate $\langle\dot{\varepsilon}_3\rangle$ (a^{-1}) was calculated at a triangulation station from the measured values of V_z and I. Obtained values of $\langle\dot{\varepsilon}_3\rangle$ averaged among several stations are shown in Fig. 31 along the triangulation chain (the abscissa represents the longitude). In the region eastward from 39°E, $\langle\dot{\varepsilon}_3\rangle$ had a large and negative value, the minimum being about -5×10^{-4} a^{-1}. Figure 31 also shows the average value of the surface dilatation rate $\dot{\Delta}$, that is $\dot{\varepsilon}_1+\dot{\varepsilon}_2$, and the sum of $\dot{\varepsilon}_1+\dot{\varepsilon}_2$ and $\langle\dot{\varepsilon}_3\rangle$. This sum gives the volume dilatation, if $\dot{\varepsilon}_1+\dot{\varepsilon}_2$ can be assumed to be constant with depth. The values $\dot{\varepsilon}_1+\dot{\varepsilon}_2+\langle\dot{\varepsilon}_3\rangle$ were in a range from 0 to -3×10^{-4} a^{-1}, which showed contraction.

The negative volume dilatation $\dot{\varepsilon}_1+\dot{\varepsilon}_2+\langle\dot{\varepsilon}_3\rangle$ was considered to have resulted from the contraction of the ice sheet along the vertical direction. It must be due mostly to densification of the upper snow layers. If so, the total amount of densification rate w (m a^{-1}) of the snow layers can be given by

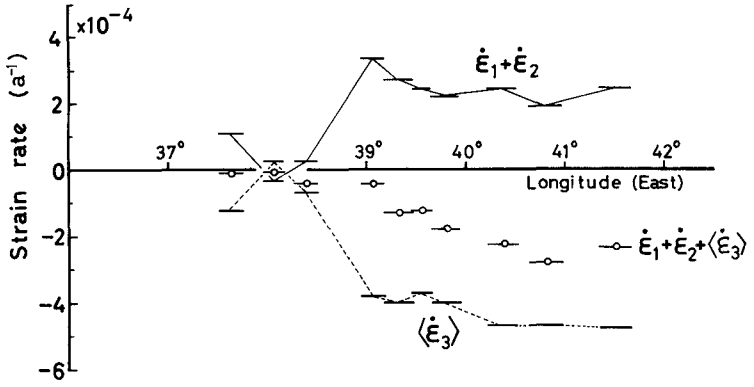

Fig. 31 Variations in surface dilatation rate $\dot{\varepsilon}_1+\dot{\varepsilon}_2$, vertical strain rate $\langle\dot{\varepsilon}_3\rangle$ and volume dilatation rate $\dot{\varepsilon}_1+\dot{\varepsilon}_2+\langle\dot{\varepsilon}_3\rangle$ per year along the triangulation chain. Each segment represents the average value over several stations.

$$w=(\dot{\varepsilon}_1+\dot{\varepsilon}_2+\langle\dot{\varepsilon}_3\rangle)I$$
$$=(\dot{\varepsilon}_1+\dot{\varepsilon}_2)I+\langle\dot{\varepsilon}_3\rangle I$$
$$=(\dot{\varepsilon}_1+\dot{\varepsilon}_2)I+V_z. \tag{18}$$

The value of w is taken negative here, and the negative value of V_z represents the downward velocity (submergence velocity). The value of w calculated from eq. (18) seemed to be somewhat too large in the absolute value, i.e., about -0.5 m a^{-1} in the region eastward from 40°E. It might be due to errors included in each term of eq. (18), and also due to the assumption of the constant strain rates with depth. However, the relation in eq. (18) is still useful, because the equation shows that an emergence (submergence) velocity taking account of the densification rate of snow layer, namely $-(V_z-w)$, should be given as the product of the surface dilatation rate $\dot{\varepsilon}_1+\dot{\varepsilon}_2$ and the ice thickness I. Then, from eqs. (12) and (18), the local net mass budget B_n is represented as

$$B_n=A_n\rho_s-(\dot{\varepsilon}_1+\dot{\varepsilon}_2)I\rho_i \ , \tag{19}$$

which is obtained without using the velocity V_z.

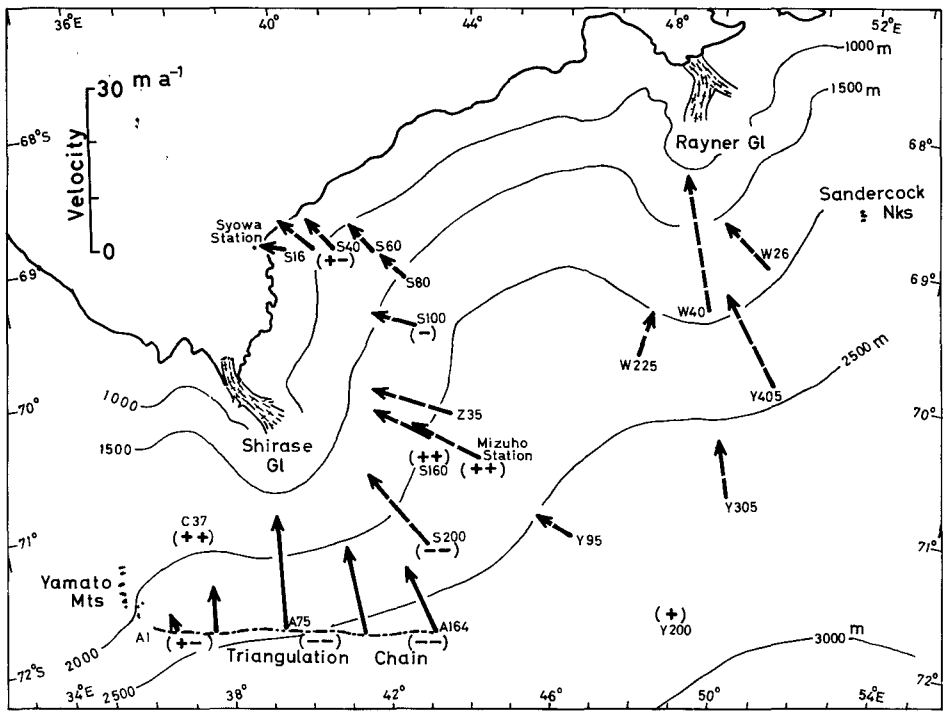

Fig. 32 Distribution of estimated local mass budgets (by marks of + or − ; see text) and predicted horizontal velocities (by arrows in broken lines) over Mizuho Plateau. Arrows in solid lines show measured velocities.

The local mass budget could, therefore, be estimated from the measured results of the surface dilatation rate, ice thickness and annual net accumulation at the square strain grids of S40, S100, S160, S200, C37, Y200 and Mizuho Station. Conditions of the calculated mass budget are shown by the marks + or − in Fig. 32. They represent as follows :

(++) : Large positive budget,
(+) : Positive budget,
(+−) : Nearly zero budget,
(−) : Negative budget,
(−−) : Large negative budget.

It was found that the local mass budget in this surveyed period was largely negative in the area around 2500 m in elevation, largely positive around 2000 m, and almost in an equilibrium state in the vicinities of both the Yamato Mountains and the coast. Although the data were scarce, the condition of the ice sheet of Mizuho Plateau seemed to be unsteady in different modes from region to region. In this regard, it can be imagined that a kinematic wave is propagated (Lighthill and Whitham 1955), giving rise to propagation of perturbation of the dynamical ice condition.

Ⅶ. 3. *Estimated velocities and flow lines*

An empirical relation was derived in Sub-section V. 4. ; namely, the surface flow velocity was almost proportional to the second power of the surface slope and to the third power of the ice thickness, based on the laminar flow formula. Using the relation shown by a straight line in Fig. 25, surface velocities were roughly estimated at 15 stations distributed over Mizuho Plateau, where the data were available of the ice thickness obtained by radio echo soundings (SHIMIZU *et al.* 1972, NARUSE and YOKOYAMA 1975) and the surface slope obtained by the skyline measurements (WATANABE and AGETA 1972).

Calculated horizontal velocities are shown by arrows in broken lines in Fig. 32, together with the measured velocities by arrows in solid lines at S16 (SHIMIZU *et al.* 1975) and at several stations along the chain. The direction of an estimated flow vector was represented as normal to the surface contour line. The velocities had large values such as 18 m a^{-1} at S200, 20 m a^{-1} at Y405 and 26 m a^{-1} at the region from W31 to W49, and small values such as less than 10 m a^{-1} in the vicinity of the coast. Two main tributary flows of the Shirase Glacier are suggested, the one crossing the middle part of the triangulation chain (39°E-40°E) and the other around S200. Meanwhile, as to the Rayner Glacier, a main flow is predicted to run from a region near Y405 to the vicinity of W40. A tendency noticed in Fig. 32 that the velocity decreases along Route S towards the coast (S100–S40–S16) can be understood as caused by the effect of diverging of flow lines (see Fig. 33).

Flow lines of ice over Mizuho Plateau were determined on the following two bases :

(1) A flow line is strictly parallel with a flow vector along Route A where the direct measurements of ice flows were made by the triangulation survey.

(2) A flow line in other regions should be normal to the surface contour line of the ice sheet, which was obtained by using the elevations along the traverse routes and also the surface slopes at some stations (SHIMIZU *et al.* 1978a). This argument was mostly supported by the result in which the directions of the ice flow and of the maximum surface slope coincided with one another approximately having the standard deviation of 9 degrees on smooth slopes in the region of the triangulation chain.

Distribution of flow lines over the lower part of the Shirase drainage and its neighbouring

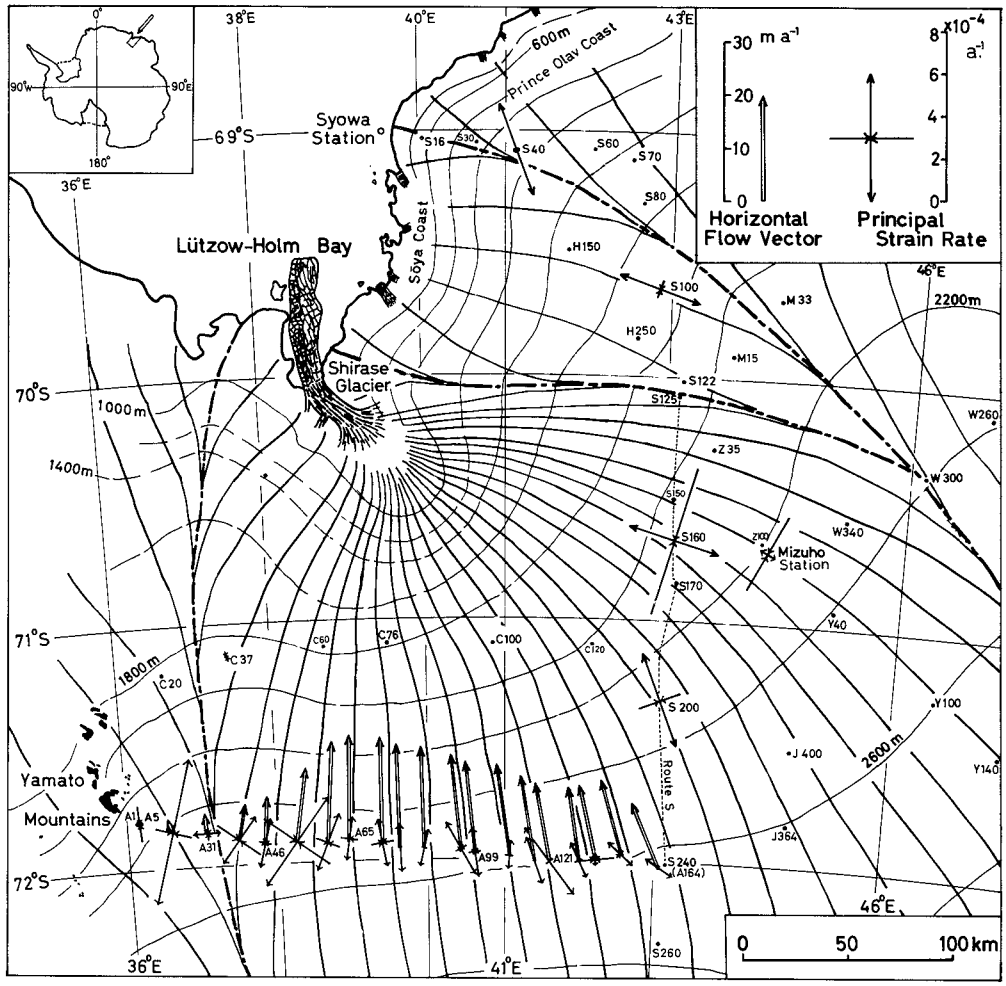

Fig. 33 Flow lines over the ice sheet of Mizuho Plateau, and distribution of horizontal vectors of ice flow and principal strain rates obtained from the triangulation chain and square strain grids. Ice divides of the drainage basins are shown by dot-dash lines. Surface contours of the ice sheet are marked every 200 m.

basins is shown in Fig. 33, together with surface flow vectors and principal strains along the triangulation chain and at S40, S100, S160, S200, C37 and Mizuho Station. It is clear from the figure that the direction of the maximum extension of surface strain was approximately parallel with the flow line. Determination of the ice divides (shown in Fig. 33) between the different drainages may be supported by the pattern of principal strains at S40, S100, and so on ; namely, stations S40 should be located in the Prince Olav drainage and S100 in the Sôya drainage.

It is also noted from the figure that the flow lines in the Shirase drainage are markedly converging into the Shirase Glacier. Features of compressive strains normal to the flow directions support the presence of converging flows, e. g., at S160, S200 and Mizuho Station. Therefore, the magnitude of surface flow velocity must increase considerably from the inland area towards the coast ; actually, the velocity was obtained to be 20 m a^{-1} at the central part of Route A and 2500 m a^{-1} at the terminus of the Shirase Glacier (NAKAWO *et al.* 1978). Horizontal velocities along a flow line from the triangulation chain in 72°S to the terminus of the Shirase Glacier in 70°S are plotted against the distance in Fig. 34, where actually measured ones are shown by solid circles while estimated ones by open circles. The ordinate is shown on a logarithmic scale. A rough calculation based on a smoothed curve in Fig. 34 showed that about 7000 years are necessary for the ice mass to travel from the triangulation chain (72°S) to the outlet of the Shirase Glacier (70°S).

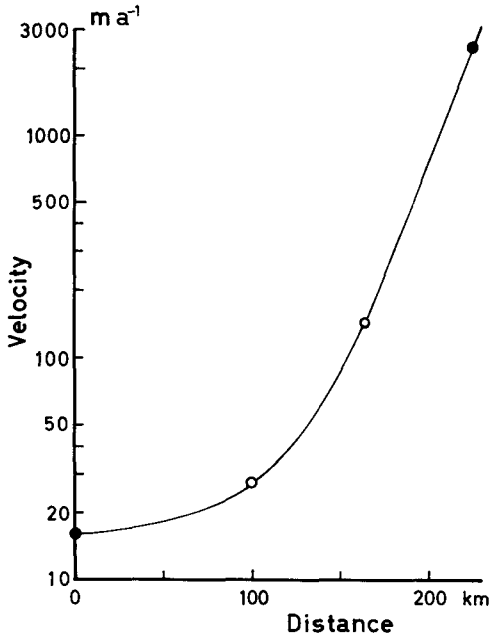

Fig. 34 Measured (●) and calculated (○) horizontal velocities along a flow line from the middle part of the triangulation chain (72°S) to the terminus of the Shirase Glacier (70°S).

The amount of ice which flows through a vertical cross section along a portion of the triangulation chain, 220 km long from the west boundary (A032) of the Shirase drainage to S240 (A164), was estimated as 4.5×10^{12} kg a^{-1}, by multiplying the cross-sectional area by the mean velocity profile estimated from the surface velocity. The amount of ice discharge obliquely across a portion of Route S (see Fig. 33), 220 km long from S240 to S124 (the north boundary of the Shirase drainage) was estimated as 3×10^{12} kg a^{-1}, using the calculated velocities shown in Fig. 32. The density of ice was taken as 900 kg m^{-3}. Then, the total of 7.5×10^{12} kg of ice flows annually towards the Shirase Glacier through the vertical section along a rectangular line, A032–S240–S124, which cuts the Shirase drainage at 2000 m–2600 m in elevation (see Fig. 33).

This amount falls just to be the same amount of ice discharge as at the terminus of the Shirase Glacier measured by means of air photographs (NAKAWO *et al*. 1978). The amount of total annual net accumulation in the region downstream from the rectangular line was estimated to be of the order of 5×10^{12} kg a^{-1}. It follows that the mass budget in the lower part of the Shirase drainage was largely positive.

VIII. Concluding remarks

Considerations of the general flow pattern of surface ice over Mizuho Plateau and discussions on the local mass budget along the triangulation chain were given in this paper together with brief descriptions of surveying procedures and methods of data reductions. Possible errors included in the results of velocity and strain rate can be regarded to be within a range of allowances for the discussion of the dynamic condition of the ice sheet, even though the chain extended as long as 250 km from the fixed reference of an ice-free rock.

Main results obtained as to ice flow, strain and local mass budget in the region along the chain in 72°S are summarized as follows :

1) The horizontal velocity has the maximum value of 20 ± 0.7 m a^{-1} in the region of 39°E-40°E.

2) The vertical velocity is downward, i. e., submergence flow, in most of the regions and amounts to -1.0 ± 0.25 m a^{-1} in the region of 40°E-42°E.

3) In the bare ice region near the Yamato Mountains, i. e., westward from 36°35′E, the horizontal velocity is smaller than 2 ± 0.1 m a^{-1}, and the vertical velocity is slightly upward, the emergence velocity being $+0.06\pm0.05$ m a^{-1}.

4) An ice divide exists at 37°E between the drainage of the Shirase Glacier and that at its west side (the Yamato Mountains area).

5) The mode of surface deformation is in general extensive along the direction of the ice flow.

6) Tensile strains are commoner than compressive ones, the mean surface dilatation rate being $+2\times10^{-4}$ a^{-1}.

7) The principal strain rate is in a range from $\pm5\times10^{-5}$ to $\pm5\times10^{-4}$ a^{-1}, except in regions where the surface undulates.

8) Direction of the ice flow coincides approximately with that of the maximum surface slope having the standard deviation of 9° on smooth surface slopes.

9) The relation $V_h \propto (\sin\theta_s)^2 \cdot I^3$ is derived empirically to estimate the velocity V_h from the surface slope θ_s and ice thickness I.

10) The net accumulation is large in the depressed terrain (mean value 0.47 m a^{-1}), small in the mound terrain (mean value 0.09 m a^{-1}), the average value in the whole area being 0.20 m a^{-1} in thickness of snow.

11) The local mass budget is approximately zero, i. e., in an equilibrium state, to the west

of 39°E, whereas to the east of 39°E it has large negative values from -500 to -800 kg $m^{-2}a^{-1}$, which signifies a considerable mass deficit.

From the above results, the following are deduced concerning the dynamic conditions of the ice sheet in Mizuho Plateau :

12) The surface velocity may not exceed 25 m a^{-1} in the inland area above 2000 m in elevation.

13) Positive and negative local mass budgets distribute over the entire region in different modes, from which it follows that the ice sheet is in an unsteady state.

14) The total ice flow across the middle part of the Shirase drainage amounting to 7.5×10^{12} kg a^{-1} is approximately the same as the total discharge of ice from the Shirase Glacier, from which it follows that the total mass budget in the lower area of the drainage is positive, nearly equal to the amount of the total annual net accumulation in the area.

15) It takes about 7×10^3 years for the ice mass to flow down from the region of 72°S to the outlet of the Shirase Glacier.

Two important problems are visualized here in regard to the dynamics of the ice sheet in Mizuho Plateau : firstly, whether the basal ice is melting or not ; secondly, how the ice sheet responds to a change in an income mass.

Based on the equation of mass continuity along a flow line, the basal sliding velocity can be estimated using the data from the chain. MAE and NARUSE (1978) showed the calculated velocity at the base as about 10 m a^{-1} in the eastern region from 39°E. This velocity is likely insofar as the basal ice is at the temperature of pressure melting point. It has been reported from the various regions of the Antarctic ice sheet that water exists at the bed (e. g., UEDA and GARFIELD 1968, OSWALD and ROBIN 1973). MAE (1978) suggested the possibility of the existence of a sub-ice water lake along a deep valley beneath Mizuho Plateau. This question remains unsolved pending a future study, awaiting information to reveal the temperature profile of the ice sheet.

The movement of the ice sheet varies as the ice mass changes. A discussion on the response of a glacier dynamics to a variation in the income mass was theoretically developed by NYE (1960) on the basis of the flow law of ice. The response time t was given approximately by $t=(4\,\mathrm{d}V/\mathrm{d}x)^{-1}$, where $\mathrm{d}V/\mathrm{d}x$ is a longitudinal strain rate (a^{-1}). Applying this equation to the ice sheet of the Shirase drainage, the response time was presumed as 1000~5000 years, whereby the discharge at the current time through the Shirase Glacier is considered as a reflection of the ice mass of the basin in the past of the order of 10^3 years ago. This long time scale should be kept in mind, when one discusses the budget of a large ice mass. The income mass, i. e., total net accumulation, actually varies considerably from year to year, as shown by YAMADA *et al*. (1978). It would fluctuate with various lapses of time from short to long years caused by variations in the climate. On the other hand, the outgo mass, i. e., the discharge of

ice through an outlet glacier, measured even only for a few years, could be valid for a considerably long term, as the movement of the ice sheet would be fairly steady except when it surges. And it takes long years for the discharge to adjust its amount with the change of accumulation.

To elucidate these problems of the ice sheet behaviour, a more sufficient knowledge is greatly called for especially as to the flow rates along a flow line and along a vertical direction, together with the thermal regime of the ice sheet.

Acknowledgements

The author is deeply indebted to many members of the wintering parties of the 10th and the 14th Japanese Antarctic Research Expedition led by Dr. K. Kusunoki and Dr. T. Hirasawa respectively, for generous support in the field. Special thanks are due to Mr. H. Ando, Dr. M. Yoshida, Dr. K. Omoto, Messrs. Y. Ageta, S. Kobayashi, Y. Abe, K. Yokoyama and K. Shiraishi for their cooperation with him in carrying out triangulation surveys, and also to the staffs of the Geographical Survey Institute, Ministry of Construction, for their net-adjustment computation of the data from the surveys of the triangulation chain by the computer NEAC-2260 located at the Institute. He also expresses his gratitude to Dr. T. Ishida, Dr. G. Wakahama, Dr. Y. Suzuki and Dr. N. Maeno of the Institute of Low Temperature Science, Hokkaido University, for reading and criticizing the manuscript of this paper, and to Dr. H. Shimizu of the same Institute, Dr. A. Higashi of Faculty of Engineering, Hokkaido University, Dr. C. F. Raymond of University of Washington, and Dr. S. Mae of National Institute of Polar Research for their helpful advice and useful comments concerning this study.

References

ABE, Y. 1975a Gravity data. Glaciological Research Program in Mizuho Plateau-West Enderby Land, East Antrarctica, Part 3, 1973-1974. *JARE Data Rep.,* **28** (Glaciology), 114-119.

ABE, Y. 1975b Geomagnetic data. Glaciological Research Program in Mizuho Plateau-West Enderby Land, East Anatarctica, Part 3, 1973-1974. *JARE Data Rep.,* **28** (Glaciology), 120-121.

ABE, Y., YOSHIMURA, A. and NARUSE, R. 1978. Gravity anomalies and bedrock relief in Mizuho Plateau. Glaciological Studies in Mizuho Plateau, East Antarctica, 1969-1975. *Mem. Natl Inst. Polar Res.,* Spec. Issue, **7**, 37-43.

AGETA, Y. and FUKUSHIMA, Y. 1972 Surface meteorological data of the Mizuho Plateau-West Enderby Land area, East Antarctica, 1969-1971. Glaciological Research Program in Mizuho Plateau-West Enderby Land, Part 1, 1969-1971. *JARE Data Rep.,* **17** (Glaciology), 135-167.

AGETA, Y. and NARUSE, R. 1971 Measurements of ice flow around Skallen Rock, south of Syowa Station, Antarctica. *Antarctic Record,* **42**, 61-64.

BADER, H. 1960 Theory of densification of dry snow on high polar glaciers. *CRREL Res. Rep.,* **69**, 1-8.

BADER, H. 1962 Theory of densification of dry snow on high polar glaciers, II. *CRREL Res. Rep.,* **108**, 1-18.

BARDIN, V. I. and SUYETOVA, I. A. 1967 Basic morphometric characteristics for Antarctica and budget of the Antarctic ice cover. *Pro. Symp. Pacific-Antarctic Sci., JARE Scientific Rep.,* Spec. Issue, **1**, 92-100.

BUDD, W. 1966 The dynamics of the Amery Ice Shelf. *J. Glaciol.,* **6**, No. 45, 335-358.

BUDD, W. 1968 The Wilks Ice Cap Project. *Proceedings of International Symposium on Antarctic Glaciological Exploration* (ISAGE), Hanover, New Hampshire, USA. Publ., **86**, 414-429.

BUTKOVICH, T. R. and LANDAUER, J. K. 1960 Creep of ice at low stresses. *SIPRE Res. Rep.,* **72**, 1-6.

CLOUGH, J. W. and BENTLEY, C. R. 1970 Measurements of electromagnetic wave velocity in the East Antarctic ice sheet. *Proceedings of International Symposium on Antarctic Glaciological Exploration* (ISAGE), Hanover, New Hampshire, USA. Publ., **86**, 115-128.

DOAKE, C. S. M. 1975 Glacier sliding measured by a radio-echo technique. *J. Glaciol.,* **15**, No. 73, 89-93.

DOAKE, C. S. M., GORMAN, M. and PATERSON, W. S. B. 1976 A further comparison of glacier velocities measured by radio-echo and survey methods. *J. Glaciol.,* **17**, No. 75, 35-38.

DORRER, E., HOFMANN, W. and SEUFERT, W. 1969 Geodetic results on the Ross Ice Shelf survey expeditions, 1962-63 and 1965-66. *J. Glaciol.,* **8**, No. 52, 67-90.

DREWRY, D. J. 1975 Comparison of electromagnetic and seismic-gravity ice thickness measurements in east Antarctica. *J. Glaciol.,* **15**, No. 73, 137-150.

FEDERER, B., SURY, H., PHILBERTH, K. and QUERVAIN, M. de 1970 Outflow and accumulation of ice in Jarl-Joset Station, Greenland. *J. Geophy. Res.,* **75**, No. 24, 4567-4569.

FEDERER, B. and SURY, H. 1976 Deducing thickness changes of an ice sheet : comments on the paper by J. F. NYE. *J. Glaciol.,* **17**, No. 77, 531.

FUJIWARA, K. and YOSHIDA, Y. 1972 Ice flow measurements on the east-coast of Lützow-Holm Bay, Antarctica. *Antarct. Rec.,* **44**, 79-92 (in Japanese).

GIOVINETTO, M. B. 1964 The drainage systems of Antarctica : Accumulation. *Antarctic Snow and Ice Studies, Antarc. Res,* Ser. **2**, Am. Geophys. Union, 127-155.

GIOVINETTO, M. B. 1968 The Antarctic ice sheet and its probable bi-modal response to climate. *Proceedings of International Symposium on Antarctic Glaciological Exploration* (ISAGE), Hanover, New Hampshire, USA. Publ., **86**, 347-358.

GLEN, J. W. 1955 The creep of polycrystalline ice. *Proc. Roy. Soc.,* **A, 228**, 519-538.

GUDMANDSEN, P. 1975 Layer echoes in polar ice sheets. *J. Glaciol.,* **15**, No. 73, 95-101.

HARADA, T. 1966 Universal program to be used with electronic computer for net-adjustment of any geodetic figure. *Bull. Geogr. Surv. Inst.,* **12**, Part 1, 21-39.

HUGHES, T. 1973 Is the west antarctic ice sheet disintegrating? *J. Geophy. Res.,* **78**, No. 33, 7884-7910.

ISHIDA, T. 1962 Seismic observation of the Yamato Mountains traversing trip. *Antarct. Rec.,* **14**, 1156-1163 (in Japanese).

JAEGER, J. C. 1969 Elasticity, fracture and flow : with engineering and geological applications. 3rd edition, Methuen & Co LTD and Science Paperbacks, London, P. 268.

KOBAYASHI, S. 1975 Meteorological data. Glaciological Research Program in Mizuho Plateau-West Enderby Land, East Antarctica, Part 3, 1973-1974. *JARE Data Rep.,* **28** (Glaciology), 83-113.

LIGHTHILL, M. J. and WHITHAM, G. B. 1955 On kinematic waves. II. A theory of traffic flow on long crowded roads. *Proc. Roy. Soc.,* **A, 229**, 317-345.

LOEWE, F. 1967 The water budget in Antarctica. *Proc. Symp. Pacific-Antarctic Sci., JARE Scientific Rep.,* Spec. Issue, **1**, 101-110.

MAE, S. 1978 The bedrock topography deduced from multiple radar echoes observed in the Mizuho Plateau, East Antarctica. *Antarct. Rec.,* **61**, 23-31.

MAE, S. and NARUSE, R. 1978 Possible causes of ice sheet thinning in the Mizuho Plateau. *Nature,* **273**, No. 5660, 291-292.

MATSUMOTO, Y. 1978 Collection of Yamato Meteorites, East Antarctica in November and December 1975, and January 1976. *Proceedings of the Second Symposium on Yamato Meteorites. Mem. Natl Inst. Polar Res.,* Spec. Issue, **8**, 38-50.

MELLOR, M. 1959a Ice flow in Antarctica. *J. Glaciol,* **3**, No. 25, 377-386.

MELLOR, M. 1959b Mass balance studies in Antarctica. *J. Glaciol.,* **3**, No. 26, 522-533.

NAGATA, T. 1978 A possible mechanism of concentration of Meteorites within the Meteorite Ice Field in Antarctica. *Proceedings of the Second Symposium on Yamato Meteorites. Mem. Natl Inst. Polar Res.,* Spec. Issue, **8**, 70-92.

NAKAWO, M., AGETA, Y. and YOSHIMURA, A. 1978 Discharge of ice across the Sôya Coast. Glaciological Studies in Mizuho Plateau, East Antarctica, 1969-1975. *Mem. Natl Inst. Polar Res.,* Spec. Issue, **7**, 235-244.

NARITA, H. and MAENO, N. 1978 Compiled density data from cores drilled at Mizuho Station. Ice-coring Project at Mizuho Station, East Antarctica, 1970-1975. *Mem. Natl Inst. Polar Res.,* Spec. Issue, **10**, 136−158.

NARUSE, R. 1975a Movement of the ice sheet observed by a triangulation chain. Glaciological Research Program in Mizuho Plateau-West Enderby Land, East Antarctica, Part 3, 1973-1974. *JARE Data Rep.,* **28** (Glaciology), 48-61.

NARUSE, R. 1975b Density and hardness of snow in Mizuho Plateau in 1969-1970. Glaciological Research Program in Mizuho Plateau-West Enderby Land, East Antarctica, Part 2, 1969-1973. *JARE Data Rep.,* **27** (Glaciology), 180-186.

NARUSE, R. 1978 Surface flow and strain of the ice sheet measured by a triangulation chain in Mizuho Plateau. Glaciological Studies in Mizuho Plateau, East Antarctica, 1969-1975. *Mem. Natl Inst. Polar Res.,* Spec. Issue, **7**, 198-226.

NARUSE, R. 1979 Dynamical features of the Meteorite Ice Field, Antarctica. *Proceedings of the Third Symposium on Yamato Meteorites. Mem. Natl Inst. Polar Res.,* Spec. Issue, **12** (in press).

NARUSE, R. and SHIMIZU, H. 1978 Flow line of the ice sheet over Mizuho Plateau. Glaciological Studies in Mizuho Plateau, East Antarctica, 1969-1975. *Mem. Natl Inst. Polar Res.,* Spec. Issue, **7**, 227-234.

NARUSE, R. and YOKOYAMA, K. 1975 Position, elevation and ice thickness of stations. Glaciological Research Program in Mizuho Plateau-West Enderby Land, East Antarctica, Part 3, 1973-1974. *JARE Data Rep.,* **28** (Glaciology), 7-47.

NARUSE, R., YOSHIMURA, A. and SHIMIZU, H. 1972 Installation of a triangulation chain and a traverse survey line on the ice sheet in the Mizuho Plateau-West Enderby Land area, East Antarctica, 1969-1970. Glaciological Research Program in Mizuho Plateau-West Enderby Land, Part 1, 1969-1971. *JARE Data Rep.,* **17** (Glaciology), 111-131.

NISHIO, F. and MAE, S. 1979 Temperature profile in the bare ice area near the Yamato Mountains. *Proceedings of the Third Symposium on Yamato Meteorites. Mem. Natl Inst. Polar Res.,* Spec. Issue, **12** (in press).

NYE, J. F. 1952 The mechanics of glacier flow. *J. Glaciol.,* **2**, No. 12, 82-93.

NYE, J. F. 1960 The response of glaciers and ice-sheets to seasonal and climatic changes. *Proc. Roy. Soc.,* **A, 256**, 559-584.

NYE, J. F. 1975 Deducing thickness changes of an ice sheet from radio-echo and other measurements. *J. Glaciol.,* **14**, No. 70, 49-56.

NYE, J. F., KYTE, R. G. and THRELFALL, D. C. 1972 Proposal for measuring the movement of a large ice sheet by observing radio echoes. *J. Glaciol.,* **11**, No. 63, 319-325.

OSWALD, G. K. A. 1975 Investigation of sub-ice bedrock characteristics by radio-echo sounding. *J. Glaciol.,* **15**, No. 73, 75-87.

OSWALD, G. K. A. and ROBIN, G. de Q. 1973 Lakes beneath the Antarctic ice sheet. *Nature,* **245**, 251-254.

PATERSON, W. S. B. 1969 The physics of glaciers. Pergamon Press, New York, P. 250.

PATERSON, W. S. B. 1976 Vertical strain-rate measurements in an Arctic ice cap and deductions from them. *J. Glaciol.*, **17**, No. 75, 3-12.

ROBIN, G. de Q. 1975 Radio-echo sounding : glaciological interpretations and applications. *J. Glaciol.*, **15**, No. 73, 49-64.

ROBIN, G. de Q. 1976 Reconciliation of temperature-depth profiles in polar ice sheets with past surface temperatures deduced from oxygen-isotope profiles. *J. Glaciol.*, **16**, No. 74, 9-22.

ROBINSON, E. S. 1966 On the relationship of ice-surface topography to bed topography on the south polar plateau. *J. Glaciol.*, **6**, No. 43, 43-54.

SATOW, K. 1977 Resurvey of strain grids at Mizuho Camp and Y200. Glaciological Research Program in Mizuho Plateau-West Enderby Land, East Antarctica, Part 4, 1974-1975. *JARE Data Rep.*, **36** (Glaciology), 139-141.

SHIMIZU, H. 1978 Outline of the studies of the Glaciological Research Program in Mizuho Plateau, East Antarctica, 1969-1975. Glaciological Studies in Mizuho Plateau, East Antarctica, 1969-1975. *Mem. Natl Inst. Polar Res.*, Spec. Issue, **7**, 1-13.

SHIMIZU, H., NARUSE, R., OMOTO, K. and YOSHIMURA, A. 1972 Position of stations, surface elevation and thickness of the ice sheet, and snow temperature at 10 m depth in the Mizuho Plateau-West Enderby Land area, East Antarctica, 1969-1971. Glaciological Research Program in Mizuho Plateau-West Enderby Land, Part 1, 1969-1971. *JARE Data Rep.*, **17** (Glaciology), 12-37.

SHIMIZU, H., WATANABE, O., KOBAYASHI, S., YAMADA, T., NARUSE, R. and AGETA, Y. 1978b Glaciological aspects and mass budget of the ice sheet in Mizuho Plateau. Glaciological Studies in Mizuho Plateau, East Antarctica, 1969-1975. *Mem. Natl. Inst. Polar Res.*, Spec. Issue, **7**, 264-274.

SHIMIZU, H., YOSHIMURA, A., NARUSE, R., WATANABE, O., NAKAWO, M. and OKUHIRA, F. 1975 Movement of ice sheet and glaciers in Sôya Coast in 1969-1972. Glaciological Research Program in Mizuho Plateau-West Enderby Land, East Antarctica, Part 2, 1969-1973. *JARE Data Rep.*, **27** (Glaciology), 162-174.

SHIMIZU, H., YOSHIMURA, A., NARUSE, R. and YOKOYAMA, K. 1978a Morphological feature of the ice sheet in Mizuho Plateau. Glaciological Studies in Mizuho Plateau, East Antarctica, 1969-1975. *Mem. Natl Inst. Polar Res.*, Spec. Issue, **7**, 14-25.

SHIRAISHI, K., NARUSE, R. and KUSUNOKI, K. 1976 Collection of Yamato meteorites, Antarctica, in December 1973. *Antarct. Rec.*, **55**, 49-60.

SWITHINBANK, C. 1968 Ice movement in the McMurdo Sound area of Antarctica. *Proceedings of International Symposium on Antarctic Glaciological Exploration* (ISAGE). Hanover, New Hampshire, USA. Publ., **86**, 472-487.

THOMAS, R. H. 1976 Thickening of the Ross Ice Shelf and equilibrium state of the West Antarctic ice sheet. *Nature*, **259**, 180-183.

THOMAS, R. H. and EILERS, D. H. 1975 Glaciological measurements on the Ross Ice Shelf. *Antarct. J.*, **10**, No. 4, 149-150.

UEDA, H. T. and GARFIELD, D. E. 1968 Deep-core drilling program at Byrd Station (1967-1968). *Antarct J.*, **3**, No. 4, 111-112.

WALFORD, M. E. R. 1972 Glacier movement measured with a radio echo technique. *Nature*, **239**, No. 5367, 93-95.

WATANABE, O. 1975 Density and hardness of snow in Mizuho Plateau-West Enderby Land in 1970-1971. Glaciological Research Program in Mizuho Plateau-West Enderby Land, East Antarctica, Part 2, 1969-1973. *JARE Data Rep.*, **27** (Glaciology), 187-235.

WATANABE, O. and AGETA, Y. 1972 Surface condition of the ice sheet in the Mizuho Plateau-West Enderby Land area, East Antarctica, 1969-1971. Glaciological Research Program in Mizuho

Plateau-West Enderby Land, Part 1, 1969-1971. *JARE Data Rep.,* **17** (Glaciology), 48-76.
WEERTMAN, J. 1976 Glaciology's grand unsolved problem. *Nature,* **260**, No. 5549, 284-286.
WHILLANS, I. M. 1973 State of equilibrium of the West Antarctic inland ice sheet. *Science,* **182**, 476-479.
WHILLANS, I. M. 1976a Radio-echo layers and the recent stability of the West Antarctic ice sheet. *Nature,* **264**, No. 5582, 152-155.
WHILLANS, I. M. 1976b The equation of continuity and its application to the ice sheet near "Byrd" Station, Antarctica. *J. Glaciol.,* **18**, No. 80, 359-371.
YAMADA, T., OKUHIRA, F., YOKOYAMA, K. and WATANABE, O. 1978 Distribution of accumulation measured by the snow stake method. Glaciological Studies in Mizuho Plateau, East Antarctica, 1969-1975. *Mem. Natl Inst. Polar Res.,* Spec. Issue, **7**, 125-139.
YAMADA, T. and WATANABE, O. 1978 Estimation of mass input in the Shirase and the Sôya drainage basins in Mizuho Plateau. Glaciological Studies in Mizuho Plateau, East Antarctica, 1969-1975. *Mem. Natl Inst. Polar Res.,* Spec. Issue, **7**, 182-197.
YANAI, K. 1978 Yamato-74 Meteorites collection, Antarctica from November to December 1974. *Proceedings of the Second Symposium on Yamato Meteorites. Mem. Natl Inst. Polar Res.,* Spec. Issue, **8**, 1-37.
YOKOYAMA, K. 1975 Net accumulation by stake measurements. Glaciological Research Program in Mizuho Plateau-West Enderby Land, East Antarctica, Part 3, 1973-1974. *JARE Data Rep.,* **28** (Glaciology), 62-82.
YOKOYAMA, K. 1978 Distribution of surface structures of the ice sheet in Mizuho Plateau. Glaciological Studies in Mizuho Plateau, East Antarctica, 1969-1975. *Mem. Natl Inst. Polar Res.,* Spec. Issue, **7**, 26-36.
YOSHIDA, M., ANDO, H., OMOTO, K., NARUSE, R. and AGETA, Y. 1971 Discovery of meteorites near Yamato Mountains, East Antarctica. *Antarct. Rec.,* **39**, 62-65.
YOSHIDA, M. and YOSHIMURA, A. 1972a Gravimetric survey in the Mizuho Plateau-West Enderby Land area, East Antarctica, 1969-1971. Glaciological Research Program in Mizuho Plateau-West Enderby Land, Part 1, 1969-1971. *JARE Data Rep.,* **17** (Glaciology), 168-203.
YOSHIDA, M. and YOSHIMURA, A. 1972b Geomagnetic survey in the Mizuho Plateau-West Enderby Land area, East Antarctica, 1969-1971. Glaciological Research Program in Mizuho Plateau-West Enderby Land, Part 1, 1969-1971. *JARE Data Rep.,* **17** (Glaciology), 204-217.